

NUMERICAL MODELING AND SIMULATION OF BULK HETEROJUNCTION ORGANIC SOLAR CELL CONSIDERING ELECTRIC FIELD DEPENDENT CARRIER MOBILITY

A thesis submitted in partial fulfillment of the requirements for the degree of
Master of Science in Electrical and Electronic Engineering

Submitted By

Mohammad Abu Raihan Miah

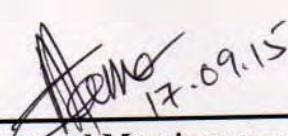


**DEPARTMENT OF ELECTRICAL AND ELECTRONIC ENGINEERING
BANGLADESH UNIVERSITY OF ENGINEERING AND TECHNOLOGY
DHAKA-1000, BANGLADESH**

September, 2015

The thesis entitled “Numerical Modeling and Simulation of Bulk Heterojunction Organic Solar Cell Considering Electric Field Dependent Carrier mobility” submitted by Mohammad Abu Raihan Miah, Roll No. 0413062226F, and Session: April, 2013, has been accepted as satisfactory in partial fulfilment of the requirement for the degree of **Master of Science in Electrical and Electronic Engineering (EEE)** on **September 17, 2015**.

BOARD OF EXAMINERS


17.09.15

1. Dr. Sharif Mohammad Mominuzzaman

Professor

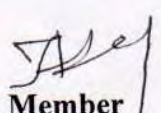
Department of Electrical and Electronic Engineering (EEE)
Bangladesh University of Engineering and Technology (BUET)
Dhaka-1000, Bangladesh

Chairman
(Supervisor)

2. Dr. Taifur Ahmed Chowdhury

Professor and Head

Department of Electrical and Electronic Engineering (EEE)
Bangladesh University of Engineering and Technology (BUET)
Dhaka-1000, Bangladesh


Member
(Ex-Officio)


17.09.15

3. Dr. Shaikh Asif Mahmood

Assistant Professor

Department of Electrical and Electronic Engineering (EEE)
Bangladesh University of Engineering and Technology (BUET)
Dhaka-1000, Bangladesh

Member


17.09.15

4. Dr. Mohammad Sharafat Hossain

Associate Professor

Department of Electrical and Electronic Engineering (EEE)
Dhaka University of Engineering and Technology (DUET)
Gazipur-1700, Bangladesh

Member
(External)

Declaration

It is hereby declared that this thesis or any part of it has not been submitted elsewhere for the award of any degree or diploma.

Author

Mohammad Abu Raihan Miah

Mohammad Abu Raihan Miah

Dedication

To
My Beloved Parents

Acknowledgements

First and foremost, I am very much grateful to the Almighty ALLAH for giving me eternal blessings on choosing the correct path towards the target of this work.

This work has been performed through inspiration and constant guidance of several kind people. Most importantly, I would like to thankfully acknowledge the help of Dr. Sharif Mohammad Mominuzzaman, Professor, Department of Electrical and Electronic Engineering (EEE), Bangladesh University of Engineering and Technology (BUET), Dhaka. His experience and in depth knowledge in the field of organic solar cell and nanotechnology, constantly guided me towards completion of the work. His guidance and insightful discussions enlightened me throughout research work. Thanks for his encouragement and trust on my ability to work on this topic. It would not be possible to complete this work without his informative assistance and guidance.

I would like to thank all the faculties, officers and staffs of my department for constant support throughout studies. Though many problems were faced at the initial stages of the work, all were overcome one by one with the help of the respected faculty members.

I am indebted to the authority of Bangladesh University of Engineering and Technology (BUET) for providing me necessary funding and good environment and facilities to complete the thesis paper.

I am grateful to my parents, my younger brother Rakib and my wife Saki for their constant support, motivation and their patience. Inspiration and cordial cooperation from friends Tanvir, Saikat, Taufiq, Ashfiq and Perthia was generous and indispensable.

Finally, author of this thesis, greatly indebted to everyone who helped throughout this work directly or indirectly, including all the members of the faculty and fellow mates of EEE department, BUET.

Abstract

Organic solar cell is one of the leading contender of the future of low cost photovoltaic cell. A great amount of experimental research has been done on this field. In this thesis, a new model for bulk heterojunction organic solar cell considering electric field dependent carrier mobility is presented for the advancement of the organic solar cell. At first, photon absorption rate, hence exciton generation rate in the active layer of organic solar cell is calculated using transfer matrix theory by taking the complex refractive index data of the organic material. AM 1.5G irradiance is taken into consideration for the calculation of photon absorption. An oscillating pattern is observed in the generation profile of the organic solar cell which can be attributed to the interference and reflectance of the layers. Generated excitons move to charge transfer state and they either dissociate or decay at the donor-acceptor interface. Exciton dissociation, decay, charge carrier generation, recombination and transport; all are incorporated in this model. As mobility is not constant for all applied voltages and electric field, so considering electric field dependent mobility is necessary to be incorporated. Variation in active layer thickness changes the electric field. Applying this model current-voltage characteristics for active layer variation from 40nm to 140 nm of a bulk heterojunction P3HT:PCBM solar cell is obtained. Open circuit voltage remains almost constant for this region, whereas both short circuit current density and efficiency follow oscillating pattern and exhibit maximum value at 60 nm. Efficiency of this bulk heterojunction organic solar cell with a 60 nm active layer is found to be 2.2%. For the bilayer structure, maximum efficiency is found to be 0.7% at 50 nm acceptor thickness. For the same structure, at lower donor thickness, efficiency is found to be higher. With the addition of a high mobility solvent carbon nano tube, 40% increase in efficiency is observed for bulk heterojunction organic solar cell. For TAPC:C60 bulk heterojunction solar cell, at 50% donor concentration efficiency is 1.05% due to reduction in dielectric constant and electron mobility. At lower concentration, efficiency and other parameter increases. For high effective density of states both open circuit voltage and short circuit current falls due to band bending near contacts. For high initial separation distance dissociation probability of exciton is high and it is observed for a variation of it.

Contents

Board of Examiners	i
Declaration	ii
Acknowledgements	iv
Abstract	v
List of Figures	viii
List of Tables	x
Abbreviations	xi
1 Introduction	1
1.1 Energy Sources	1
1.2 Solar Cells	3
1.3 Background and Present State of the Problem	4
1.4 Objectives	5
1.5 Thesis Layout	5
2 Review of Organic Solar Cell	7
2.1 Photovoltaic over the Years	7
2.2 Generation of Solar cells	9
2.3 Organic Solar Cell	11
2.3.1 Why Organic Solar Cell?	11
2.3.2 Differences Between Organic and Inorganic Solar Cell	12
2.3.3 Different Types of Organic Solar Cell	16
2.3.3.1 Bilayer Organic Solar Cell	16
2.3.3.2 Bulk Heterojunction Organic Solar Cell	17
2.3.3.3 Tandem Organic Solar Cell	17
2.3.4 Photocurrent Generation in Organic Solar Cell	18
2.3.5 Challenges	21
2.4 Different Parameters of Solar Cell	22
2.4.1 Open Circuit Voltage (V_{oc})	22
2.4.2 Short Circuit Current Density (J_{sc})	22

2.4.3	Fill Factor (FF)	23
2.4.4	Power Conversion Efficiency	23
2.5	Different Modeling Scheme for Bulk Heterojunction Organic Solar Cell	24
2.5.1	Koster Model	25
2.5.2	Analytical Model	27
2.5.3	Morphological Model	27
3	Results and Discussions	28
3.1	Performance Analysis of Bilayer Organic Solar Cell	28
3.1.1	Effect of Acceptor Layer Thickness on Device Performance	30
3.1.2	Effect of Donor Layer Thickness on Device Performance	31
3.1.3	Effect of Electron Mobility on Device Performance	33
3.1.4	Discussion	34
3.2	Modeling of Bulk Heterojunction Organic Solar Cell	34
3.2.1	Optical Modeling of Bulk Heterojunction Organic Solar Cell	35
3.2.2	Electrical Modeling of Bulk Heterojunction Organic Solar Cell	39
3.2.2.1	Exciton Dissociation in BHJ Device	40
3.2.2.2	Charge Carrier Generation, Transport and Recombination	41
3.2.2.3	Outline of Modeling	45
3.3	Results of Optical Modeling	45
3.4	Results of Electrical Modeling	48
3.4.1	Variation of Active Layer Thickness	48
3.4.2	Effect of Addition of Higher Mobility Solvent, CNT	52
3.4.3	Effect of Donor Concentration on the Device Performance	55
3.5	Sensitivity to the Parameters	58
3.5.1	Sensitivity of effective density of states	58
3.5.2	Sensitivity of Initial Separation Distance	60
4	Conclusion and Suggestions	62
4.1	Conclusion	62
4.2	Suggestions	64
A	Simulation Codes	65
A.1	Sample Code for Optical Modeling	65
A.2	Sample Code for Electrical Modeling	69
	Bibliography	81

List of Figures

1.1	Annual oil production	2
1.2	Timeline of highest efficiencies in various solar cell technology . . .	3
2.1	Chemical structure of organic material that is used in DSSC	13
2.2	Chemical structures of molecular semiconductors used in OPVs. . .	14
2.3	Chemical structures of conjugated polymers used in OPVs.	15
2.4	Difference between organic and inorganic solar cell	15
2.5	Schematic diagram and energy band diagram of heterojunction solar cell	16
2.6	Rudimentary difference between bulk and bilayer organic solar cell .	17
2.7	Photocurrent generation in organic solar cell	19
2.8	Spectral irradiance of the AM1.5G solar spectrum up to 1350 nm .	25
2.9	Koster model for the calculation of current-voltage characteristics of organic solar cell with constant carrier mobility	26
3.1	Effect of Acceptor Layer Thickness on Current-Voltage Characteristics	30
3.2	Effect of Acceptor Layer Thickness on Efficiency	31
3.3	Effect of donor layer thickness on current-voltage characteristics . .	32
3.4	Effect of donor layer thickness on efficiency	32
3.5	Effect of Electron Mobility on Current-Voltage Characteristics . . .	33
3.6	Effect of Electron Mobility on efficiency	34
3.7	Typical device structure showing optical electric field	36
3.8	BHJ solar cell structure and energy level	42
3.9	Flow chart of the proposed model	46
3.10	Generation rate of excitons in P3HT:PCBM bulk heterojunction solar cell	47
3.11	Absorption rate of different layer of P3HT:PCBM solar cell	47
3.12	J-V characteristics with a variation of active layer thickness	49
3.13	Voc with a variation of active layer thickness	49
3.14	Jsc with a variation of active layer thickness	50
3.15	Fill Factor with a variation of active layer thickness	51
3.16	Efficiency with a variation of active layer thickness	52
3.17	J-V characteristics with a variation of hole mobility	53
3.18	Open circuit voltage with a variation of hole mobility	54
3.19	Short circuit current with a variation of hole mobility	54
3.20	Fill factor with a variation of hole mobility	54

3.21	Current voltage characteristics with a variation of donor concentration	56
3.22	Open circuit voltage with a variation of donor concentration	57
3.23	Short Circuit Current with a variation of donor concentration . . .	57
3.24	Current Voltage Characteristics with a variation of effective density of states	59
3.25	Open circuit voltage with a variation of effective density of states .	59
3.26	Short circuit current with a variation of effective density of states .	60
3.27	Fill factor with a variation of effective density of states	60
3.28	Current Voltage characteristics with a variation of initial separation distance	61

List of Tables

3.1	Efficiency of solar cell with and without CNT	53
3.2	Efficiency of solar cell with donor concentration	58

Abbreviations

PV	PhotoVoltaic
SC	Solar Cell
OSC	Organic Solar Cell
OPV	Organic Photo Voltaic
CSIRO	Commonwealth Scientific and Industrial Research Organization
DSSC	Dye Sensitized Solar Cell
PHJ	Planar Hetero Junction
BHJ	Bulk Hetero Junction
TM	Transfer Matrix
FF	Fill Factor
HOMO	Highest Occupied Molecular Orbital
LUMO	Lowest Unoccupied Molecular Orbital
ITO	Indium Tin Oxide
DA	Donor Acceptor
CNT	Carbon Nano Tube
SCLC	Space Charge Limited Photocurrent
P3HT	Poly (3-hexylthiophene)
PCBM	(6,6)-Phenyl C₆₁ Butyric acid Methyl ester
PCE	Power Conversion Efficiency
PEDOT:PSS	Poly (3,4-ethylenedioxythiophene):poly(styrene sulfonate)
TOF	Time of Flight
AM 1.5	Air Mass
TAPC	1,1-bis-4-bis(4-methyl-phenyl-amino-phenyl)-cyclohexane
CT	Charge Transfer

PTCBI	3,4,9,10-perylene tetracarboxylic-bisbenzimidazole
PTCDA	Perylenetetracarboxylic dianhydride
Me-PTCDI	N,N-dimethyl-3,4,9,10-perylenetetracarboxylic acid diimide
H2Pc	free base phthalocyanine
TPyP	5,10,15,20-tetra(3-pyridyl)porphyrin
ZnPc	Zinc phthalocyanine
TPD	N,N-diphenyl-N,N-bis(3-methyl-phenyl)-[1,1-biphenyl]-4,4-diamine
CBP	4,4'-bis(carbazol-9-yl)-biphenyl
PPV	para-phenylene-vinylene
MEHPPV	poly(2-methoxy,5-(2-ethyl)-hexyloxy-p-phenylenevinylene)
CNPPV	cyano-para-phenylene-vinylene
MDMO-PPV	2-methoxy-5-(3,7-dimethyloctyloxy)-1,4-phenylene vinylene
POPT	poly((3,4-octyl)phenyl)thiophene)
EHHPPyPzV	poly(pyridopyrazine vinylene)
BBL	benzimidazo-benzophenanthroline ladder
F8BT	poly(9,9-dioctylfluorene-co-benzothiadiazole)

Chapter 1

Introduction

1.1 Energy Sources

Sun is the primary energy source which provides enormous amounts of energy powering oceans, atmospheric currents, and cycle of evaporation and drives river flow, hurricanes and tornadoes that peril our natural landscape. The devastating San Francisco earthquake of 1906 (magnitude 7.8) released an estimated 10^{17} joules of energy which sun delivers in one second. Humans use about 4.6×10^{20} joules per annum which sun supplies in one hour. Sun continuously supplies about 1.2×10^{25} terawatts of energy which is very much greater than any other renewable or non-renewable sources of energy can provide. This energy is much greater than the energy required by human beings which is about 13 terawatts. Total 0.16% of earth's land with 10% efficient solar cells would provide 20 Terawatts of energy which is accounted as about twice of fossil fuel consumption of the whole world including numerous nuclear fission reactors [1].

Human can use a little of abundance solar energy. On an account 80%-85% of our total energy comes from fossil fuels which are non-renewable, quick depleting, greenhouse gas producer and other environmental pollutants producer [2]. Emission of greenhouse gas like CO_2 by fossil fuels imbalance the ecological equivalence.

This problem can be resolved by using fossil fuels in conjunction with carbon sequestration, nuclear power and solar power. Carbon sequestration is an extremely difficult method since a large volume of space is required to store the emitted greenhouse gases and its maintenance is a very critical one. On the other hand, nuclear power seems to be a good option but the feasibility of deploying several thousands of 1 Gigawatt power plants all over the world to meet the 10 tera watt demand of the society is sceptical. The Uranium resource for these power plants also gets exhausted in this process in about 10 years after which the processing of sea water has to be adopted which is also exhaustible and difficult. On the other hand shifting the focus on renewable sources of energy is the ideal choice and solar power is by far the most prominent energy source owing to its versatility, inexhaustible and environmental friendly features [1].

The exhaustible nature of fossil fuels has also pushed us into the adoption of renewable sources of energy for the future. Figure 1.1 shows the plot of the annual production of oil vs. year with a 2% annual growth and decline rate [3].

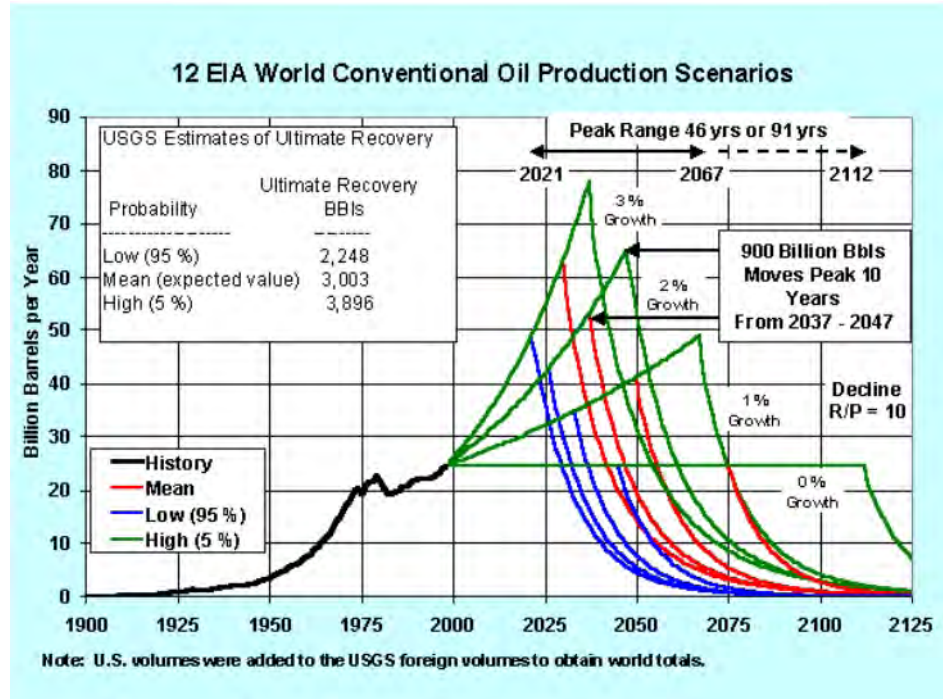


FIGURE 1.1 Annual oil production of the world. Figure is taken from [3]

High costs and conversion efficiency have been the major bottlenecks in the potential of solar power becoming a primary source of energy. Now a days, major

research done with the motive of improving the efficiency of these cells has brought this dream closer to reality. New methods of harnessing the full spectrum of the sun's wavelength, multifunction solar cells (homojunctions and heterojunctions), and new materials for making solar cells are paving way for solar power to be the emerging power resource for the world at large. Efficiencies of different solar cells that are investigated by the researcher are shown in Figure 1.2.

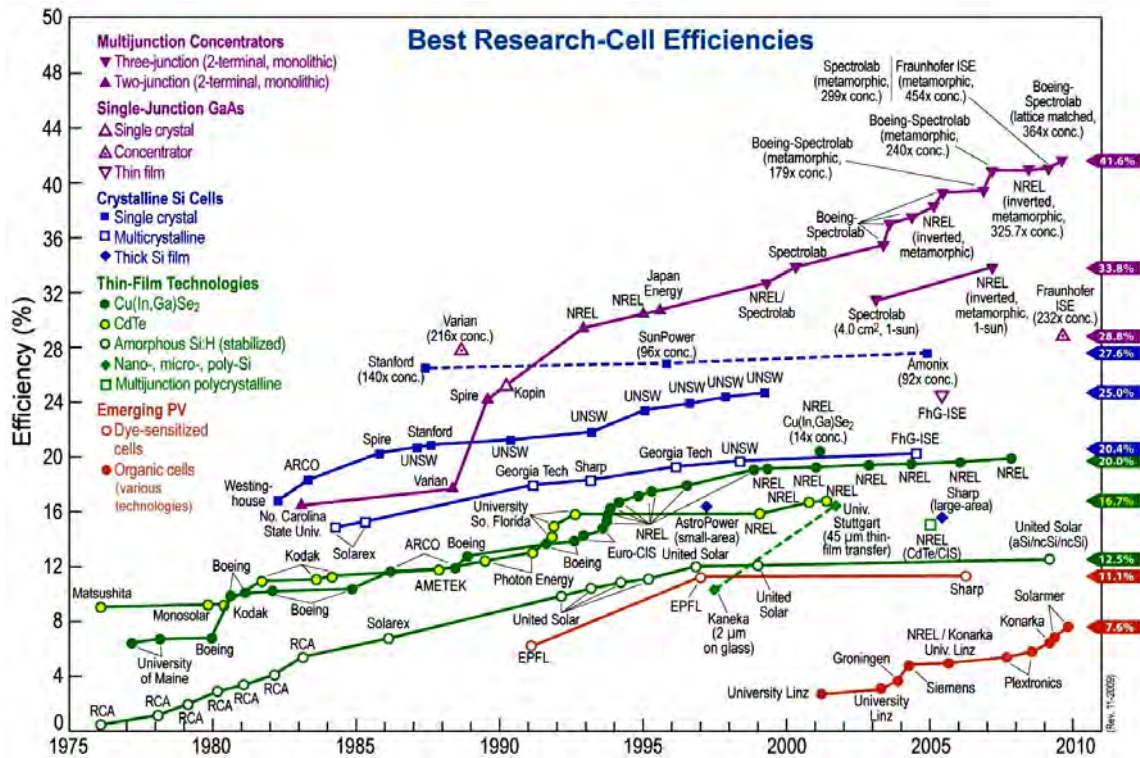


FIGURE 1.2 Timeline of highest efficiencies in various solar cell technology [4].

1.2 Solar Cells

The need to develop inexpensive renewable energy sources continues to stimulate new approaches to production of efficient, low-cost photovoltaic devices. Although inorganic semiconductors (silicon, amorphous silicon, gallium arsenide, and sulphide salts) have been the primary focus, the photosensitivity and the photovoltaic effects in devices made with organic materials have also been explored, including conjugated polymers, organic molecules, stacked discotic liquid crystals, and self-assembling organic semiconductors [5]. Because of the advantages

that would be realized with polymer-based photovoltaics (such as low-cost fabrication in large sizes and in desired shapes), efficient organic solar cells would have a major impact [6]. Solar cells or Photovoltaic cells are the device that converts the radiation of the sun to electricity. Many attempts have been done looking for a high efficiency low cost solar cells, leaving significant milestone. Organic photovoltaic cells as potential renewable energy sources are of great interest and have revealed significant potential for competition with conventional inorganic sources. These cells are fabricated from inexpensive organic materials, easy preparation methods and can be deposited on large scale [7]. The field was started by the application of small organic molecules and since the development of semiconducting polymers, these materials was incorporated into organic cells. Currently , most OPV cells have a bulk heterojunction structure composed of conjugated polymers and fullerene derivatives. The best performance achieved from a BHJ-structured OPV cell was recorded conversion efficiency of 8% [8]. On this background, organic bulk heterojunction solar cell have considered a potential source for use in Organic Photovolataic Device (OPV) devices.

1.3 Background and Present State of the Problem

Organic Solar cell is considered as an alternative of conventional solar cell due to its low fabrication cost and mechanical flexibility [9]. But as their efficiency is low compared to existing solar cell [3], a great amount of experimental research work is performed related to Organic solar cell to improve the device performance [10–12]. The performance of organic solar cell is improved by the introduction of bulk heterojunction as an active layer [13].

Modeling of organic solar cell provides an opportunity to find new device designs, examine properties that are out of reach or too expensive to measure, study numerous device structures in a very short period of time and relate the experimental result quantitatively to predict device performance. Various modeling

schemes based on Poisson-continuity equation considering constant mobility, Dynamic Monte Carlo Simulation are proposed for organic bulk heterojunction solar cells by the researchers [14–17]. A model considering both electric field dependence mobility of charge carriers and dissociation probability of excitons in active layer are necessary to consider the effect of active layer thickness on device performance. Simulation based on charge carrier density and exciton density consistency in iterations are required to be explored. Moreover, device performance with a variation of active layer thickness, with the inclusion of solvent of high mobility, with a deviation in density of states in active layer and with a change in donor concentration in active layer can result in different performance.

1.4 Objectives

The objectives of this thesis are to:

- Model organic bulk heterojunction solar cell considering both field dependent mobility of charge carrier and exciton dissociation probability with consistency of charge carrier density and exciton density.
- Find out the effect of active layer thickness of solar cell on generation rate and J-V characteristics of the device.
- Find out device J-V characteristics with the inclusion of high mobility solvent such as Carbon Nano Tube (CNT) in active layer.

1.5 Thesis Layout

The thesis has been divided into four chapters. This chapter provides general information followed by the background, present state of the problem and objectives of the thesis work.

Chapter two covers the generations of solar cell technologies, basic of a solar cell, different parameters of a solar cell, working principle of solar cell, difference between organic and inorganic solar cell, different kind of organic solar cells, photogeneration mechanism in organic solar cell and challenges of organic solar cell, different modeling schemes of solar cell. Overall chapter two gives the idea about present state of organic solar cells and different modeling schemes used for modeling them.

Chapter three covers the performance analysis of bilayer organic solar cell at first. After that field dependent carrier mobility based model is explained. In the modeling part there is two parts mainly optical modeling and electrical modeling. In the optical modeling section, transfer matrix theory is used for the calculation of photon absorption. After that electrical modeling is done considering exciton dissociation, decay, charge carrier recombination, charge carrier generation and transport. Thereafter, modeling is used to find the effect of active layer thickness, mobility and donor concentration on device performance.

Chapter four provides conclusive discussions for this work. Some scopes for the future work in relation with the present work are also presented.

Chapter 2

Review of Organic Solar Cell

2.1 Photovoltaic over the Years

The first record of the ‘photovoltaic effect’ is related to a French scientist back in 1839. Edmond Becquerel found that by the action of a beam of sunlight over two different liquids, chemically interacting and carefully superposed in a glass container and an electric current was developed, as indicated by a very sensitive galvanometer connected with two platinum plates dipping in the two different solutions [18]. But the understanding of the PV effect came about later by Albert Einstein’s paper on the photoelectric effect in 1905, which later led to him winning the Nobel Prize in 1921.

Like many other electronic devices, a relatively efficient (6%) silicon based solar cell was discovered at Bell Laboratories in 1953 and like many other scientific innovations, its discovery was accidental. Gerald Pearson, Calvin Fuller and Daryl Chapin discovered photovoltaic while they were trying to improve silicon’s conductivity [19]. Previous photovoltaic research was based on selenium, which has less efficiency and is also more expensive. Therefore, this discovery was a breakthrough for bringing PVs into everyday life. In the next year, Bell Laboratories unveiled their very first solar cell.

Later in 1955, the United States' government announced that they had a plan to launch satellites. Because of the impossibility of providing power to the satellite from earth, there was a good opportunity for PV s to show their value. Therefore, suddenly there was an application with a wealthy sponsor to support the research on PV s. Most of the later innovations and development in the solar power field happened in the Cold War years and during the adversary between Soviet Union and United States over control of space, or in a better word in the famous 'Space Rac'.

The next applications for SCs apart from the space application were related to oil rigs in the Gulf of Mexico. For security reasons it is needed for tall structures to have a blinking light on them, but once again the distance to the source of electricity made this the next job of SCs.

It is still far away from having solar cell as primary power source in every house's roof. To become compatible with other electrical sources and to become a domestic power source, two major improvements had to happen, for the solar cells:

1. The size of each unit should shrink (improvement in efficiency)
2. The cost of manufacturing should have been reduced to improve the ratio of cost per kwatt

To improve the efficiency, the quality of the materials had to be improved (better crystal quality), fabrication methods had to be reformed and new structures had to be introduced. However, all of the mentioned changes would increase the cost of manufacturing. Therefore, at the same time, researchers were trying to decrease the total cost of the solar cells by finding cheaper types of material (i.e. amorphous semiconductors, organic material and so on) or cheaper structures with lower manufacturing cost (i.e. planar SCs with printing technique as their fabrication method [9]).

For organic photovoltaic, it was in early years of 60's that researchers noticed the potential of organic materials in imaging systems [20]. During the next couple

of years, investigation in the field of organic photovoltaic (or OPV) continued but efficiencies were really low. As an example, 0.001% efficiency reported by C. W. Tang et.al. in 1975 was the state of the art. In 1977, it is discovered that the conductivity of the conjugated polymer can be increased by the range of eleven order of magnitude [21]. Later on, in 2000, they received a Nobel Prize in Chemistry because of their great works on conductivity and superconductivity in organic materials [22]. The first OSC with efficiency over 1% was reported in 1986 once again by C. W. Tang [23]. The latest development is related to Solarmer Energy Inc. On 27 July 2010, Forbes.com reported that Solarmer broke the 8% wall and reported an organic solar cell with 8.13% efficiency [24]. Forbes predicted that by this discovery, the cost of energy production for OPVs will go down to 12-15 cents/kWh.

2.2 Generation of Solar cells

Solar cells are categorized into three generations based on the order of their prominence. Research is being conducted on all the three generations concurrently to improve their efficiencies while the first generation solar cells comprise the major share of commercial production about 89.7% in 2007 [25].

Large area, high quality and single junction devices form the first generation solar cells. Reduction in production costs of this technology is nullified owing to high energy and labor costs, material costs mostly for the silicon wafer, strengthened low-iron glass cover sheet and costs of other encapsulation. This trend is continuing as the photovoltaic industry is expanding. Although it has a broad spectral absorption range, the high energy photons at the blue and violet end of the spectrum is wasted as heat [26]. Producing solar cells using high-efficiency processing sequences with high energy conversion efficiency are thus favored provided they do not increase the complexity of the solar cell. Theoretical limit on efficiency for single junction silicon solar cells i.e. 33% and this is also being reached very rapidly.

To address these problems of energy requirements and production costs of solar cells a switch from first generation to second generation of thin-film cell technology has been imminent. By eliminating the silicon wafer a major reduction in material costs have been possible in the thin-film technology. They also have an advantage of increasing the unit size from silicon (100cm^2) to glass plate (1m^2). Over time the second generation solar cells are expected to bridge the gap between them and the first generation cells with respect to energy conversion efficiency. With the increase in dominance of this technology the costs of the constituent materials also goes up for top cover and other encapsulation to give it a longer life [20]. The materials generally used in this thin film technology are cadmium telluride, copper indium gallium arsenide, amorphous silicon and micromorphous silicon. These materials reduce mass and therefore cost by forming substrates for supporting glass and ceramics. Not only do they reduce costs but also promise very high energy conversion efficiency. A trend towards shifting to second generation from first generation is showing up but the commercialization of this technology has proven to be difficult [20]. Fortunately with the development of new materials over the coming decades the future of thin-film technology seems to be promising [26]. Research for improving solar cell performance by enhancing its efficiency and pushing it closer to the thermodynamic limits has led to the development of third generation solar cells [27]. To improve upon the poor electrical performance of the thin-film technology by maintaining low production costs this technology includes among others, non semiconductor technologies (including polymer based cells and biometrics) [28].

The devices comprising the third generation solar cells are quantum dot technologies, tandem/multi junction cells, hot-carrier cells, up conversion technologies and solar thermal technologies like thermo photonics, organic solar cells. This solar cells exhibit low efficiency but can be produced at a very low cost with increased mechanical flexibility.

2.3 Organic Solar Cell

2.3.1 Why Organic Solar Cell?

Compared to conventional solar cells, organic solar cells are relatively cheaper to produce. The obvious reason is that the type of materials used in organic solar cells are less expensive, needs less preparation and is more abundant than conventional crystalline solar cells.

Organic materials are polymers and oligomers as well as organic molecules very similar to the plastic bags that we use every day. Similar to plastic bag, they are products of oil. Therefore, in the case of mass production, their price can be really low.

On the other hand, unlike conventional solar cells that are based on crystalline semiconductors, which need high purity in material and therefore, costly preparation and purification processes, organic materials that are used in organic solar cells are easy to process with very cost effective processes.

Because of malleability of organic materials, organic solar cells are capable of getting into any shape during the process of fabrication and the final production can also be a flexible sheet that can be wrapped and packed for example into a soldier's backpack and in the case of necessity for recharging an electrical equipment be unwrapped and used.

Moreover, the fabrication methods for organic solar cells are much cheaper than conventional solar cells. As an example they do not need a clean room facility for their fabrication procedure. The deposition processes in the case of molecular and polymeric thin film are spin-coating, screen printing, spray coating and ink jet coating, reel to reel printing [9], which are low cost, simple and they are also suitable for large area and ultra thin layer fabrication, which in the case of mass production make the whole process of fabrication extremely cost effective.

Furthermore, a reel to reel printing process can print 1G watt capability of solar cells with five months printing. All of the mentioned reasons and the low efficiency of organic solar cell, compared to the conventional solar cells, make the organic solar cell a prospective and interesting research topic.

2.3.2 Differences Between Organic and Inorganic Solar Cell

The first difference between organic and inorganic Solar cell (SC) is the materials that are used to make them. As it can be deduced from the names, in the inorganic SCs, inorganic materials such as crystalline materials are used. These solar cells have good electrical properties, which are mostly because of their crystalline structure. On the other hand, they have a relatively low light absorption, which can be corrected using a multi-stage structure. On the other hand, organic solar cells are made of organic materials. Organic SCs based on their materials can be divided to the following categories:

1. Dye-sensitized Organic Solar Cell
2. Molecular Solar Cell
3. Polymeric Solar Cell
4. Mixed Solar Cell

Organic dye-sensitized SCs (ODSSC) are made of a liquid electrolyte that transports generated carriers created by organic molecules inside the electrolyte. This type of OSC is very cheap but at the same time its external efficiency is really low ($< 1\%$). Figure 2.1 shows the chemical structure of organic material that are usually used in DSSCs.

Both molecular and polymeric SCs are made of non-crystalline amorphous molecules. Molecular and polymeric materials are usually used together to increase both absorption and electrical conductivity. The molecular section has better optical power absorption while polymers have a better electrical conductivity. Therefore,

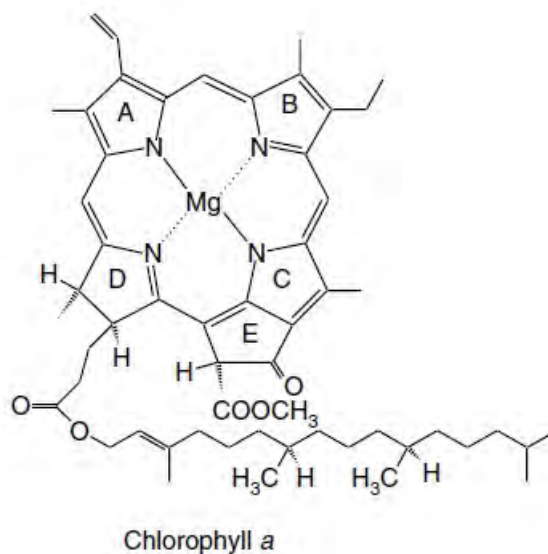


FIGURE 2.1 Chemical structure of organic material that is used in DSSC [29].

optical power is absorbed by the molecular section and electrical conductivity is provided by a network made of polymer strings.

Figure 2.2 and 2.3 respectively show the chemical structures of some molecular and polymeric materials that are used in fabrication of Organic solar cells.

Another major difference between conventional and organic SCs is due to the mechanism of charge generation and charge transport. In inorganic SCs, after the absorption of a photon, an electron is excited and an electron-hole pair is generated. Then, because of the built-in potential, they are separated from each other. After separation, because of electrostatic charges that each one of them has, electrons would be drifted towards anode and holes would be drifted towards cathode. Figure 2.4 shows a schematic depiction of a conventional SC that mimics the mechanism of charge generation inside a conventional SC. In the case of organic SCs, electron and holes are tightly bound together and make an exciton due to low dielectric constant of the organic material.

The binding energy of organics' excitons and their separation energy is a little different than conventional semiconductor excitons. In both of them coulomb attraction between the electron and hole exist and to break the exciton that barrier

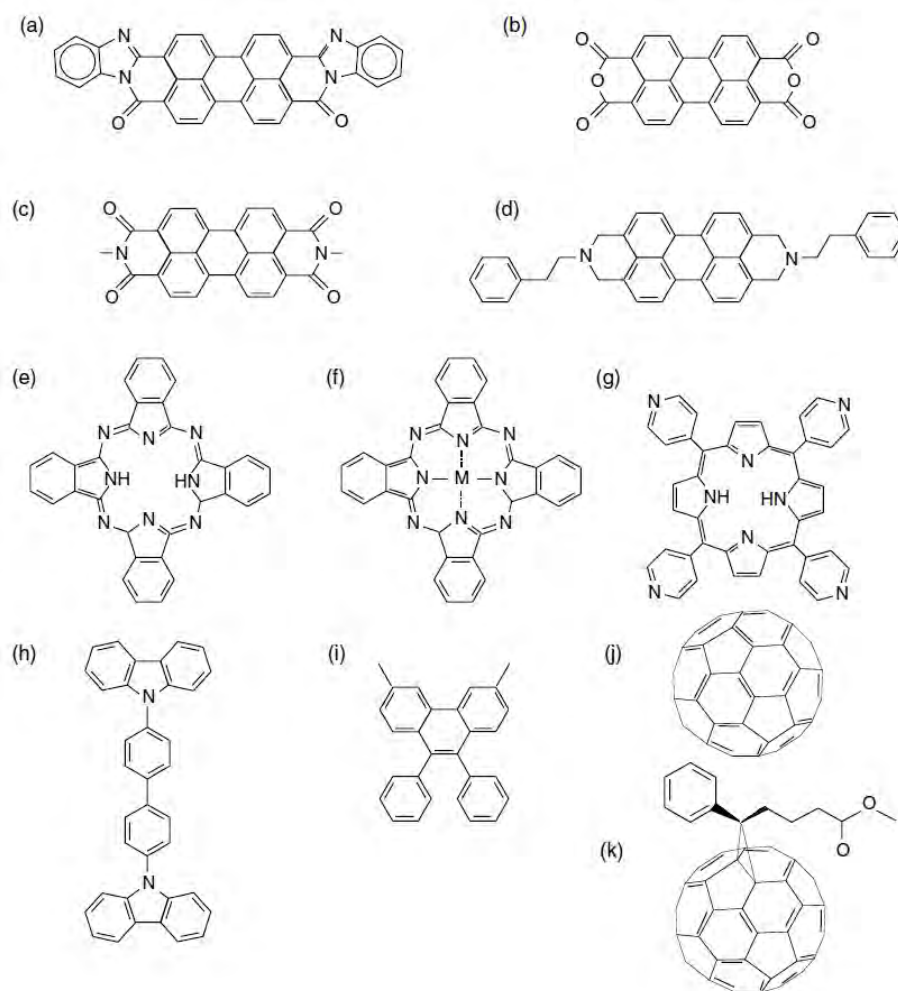


FIGURE 2.2 Chemical structures of molecular semiconductors used in OPVs. (a) PTCBI, (b) PTCDA, (c) Me-PTCDI, (d) Pe-PTCDI, (e) H2Pc, (f) MPc (MZn, Cu), (g) TPyP, (h) TPD, (i) CBP, (j) C60, (k) 5,6-PCBM [29].

of energy should be overcome. However, in the case of organic excitons, the situation is a little different. An exciton in an organic segment is one of the stable states in the discontinuous energy states of that segment and is related to a stable orbital form of electron cloud of that segment. Therefore, breaking an organic exciton is equivalent to a change in a stable state, which requires an amount of energy that is more than the coulomb attraction. Thermal excitation cannot break it.

Since an exciton has both types of charges, it cannot be attracted towards any of the electrodes due to the internal built-in potential. However, like many other particles, they can diffuse. If an exciton gets to a conductive layer, electron and hole will be recombined at the surface of that conductive layer and as a result,

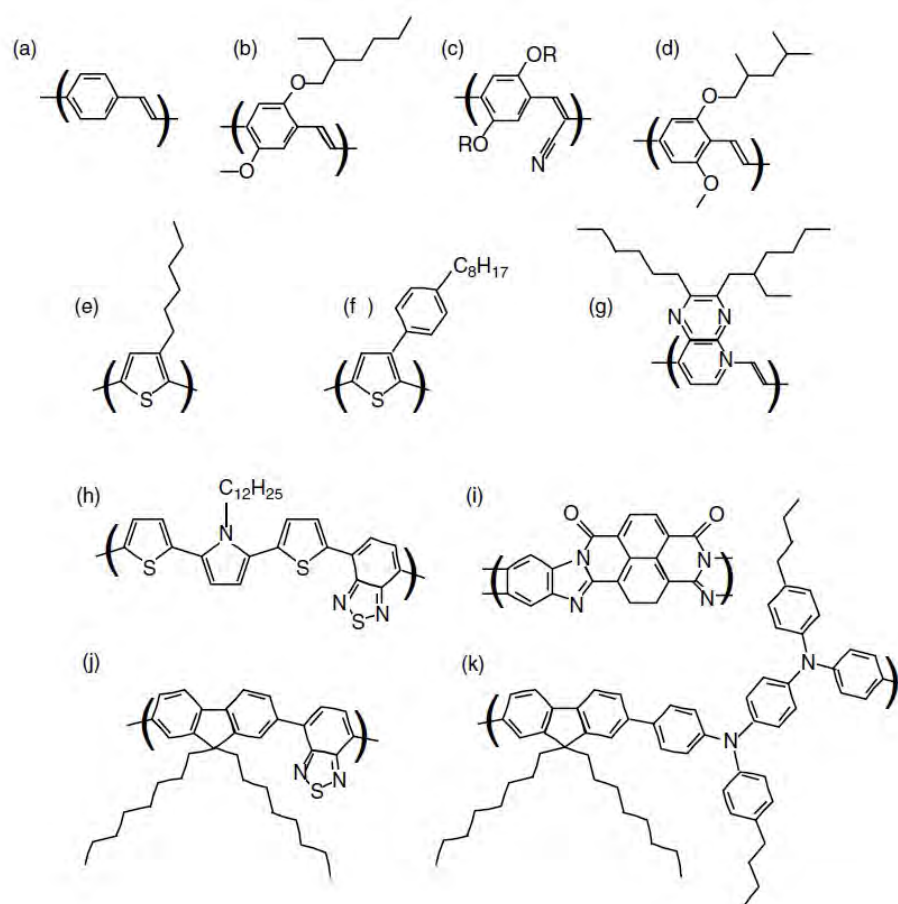


FIGURE 2.3 Chemical structures of conjugated polymers used in OPVs: (a) PPV, (b) MEHPPV, (c) CNPPV (various alkoxy cyano-derivatives have been prepared), (d) MDMO-PPV, (e) P3HT, (f) POPT, (g) EHHPPyPz, (h) PTPTB, (i) BBL, (j) F8BT, (k) PFMO [29].

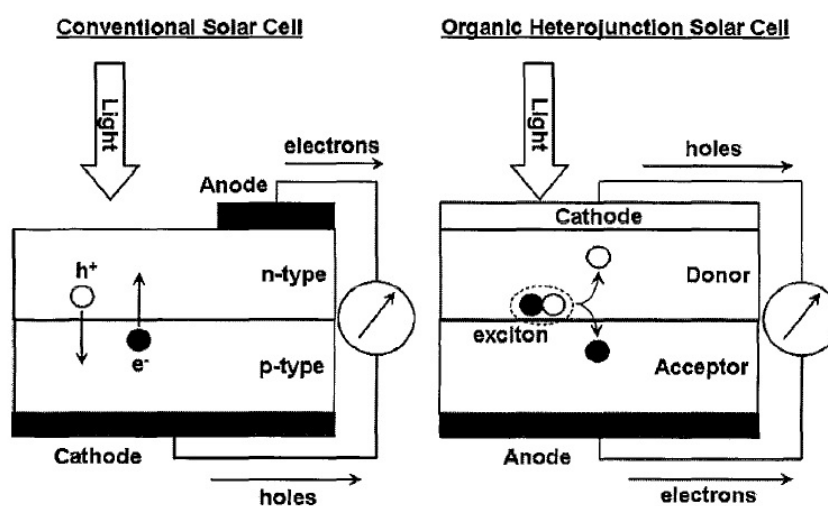


FIGURE 2.4 Difference between organic and inorganic solar cell [30].

no electrical power will be generated. Consequently, electrons and holes should be separated before that. To generate an electron-hole pair out of an exciton, one of the following conditions should exist either High electrical fields or Interface of two materials with two different energy bands.

Because of the low built-in potential in organic solar cells, using heterojunctions, the second condition is used in the structure of the OSCs to break up the excitons. In the next section, different structures of Organic solar cells are discussed.

2.3.3 Different Types of Organic Solar Cell

Two different type of organic solar cell will be discussed. One is called bilayer organic solar cell or Planar Heterojunction solar cell and another is called bulk heterojunction solar cell. Now the common structure of heterojunction solar cell is shown in Figure 2.5

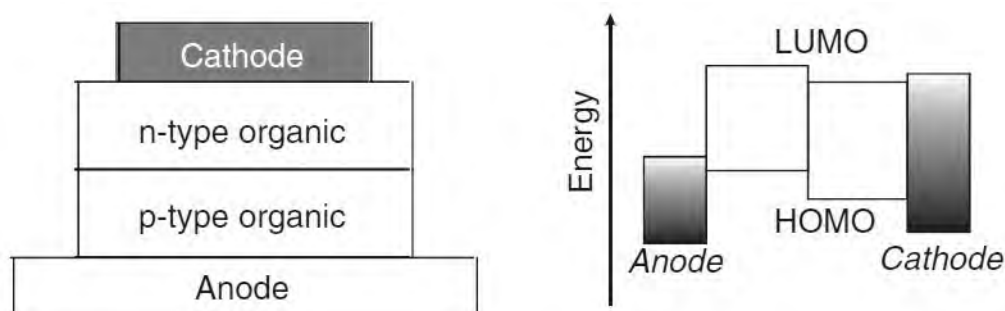


FIGURE 2.5 Schematic and energy band diagram of heterojunction solar cell[29].

2.3.3.1 Bilayer Organic Solar Cell

In this structure, by incoming light from a transparent anode an exciton is generated and it will diffuse all the way (7-10 nm) to the interface of donor and acceptor layers where they are separated into a hole and an electron. Later, these generated charges will reach the electrodes by means of drift and diffusion, and will create electrical current. Because of the exciton's short diffusion length, most of the excitons cannot make it all the way to the DA interface and a recombination will happen. Therefore, the total amount of electrical power will be reduced

and the efficiency will decrease. As a result, one way of increasing the efficiency is to fabricate very thin active layers but this may result in low optical power absorption.

2.3.3.2 Bulk Heterojunction Organic Solar Cell

One idea is to mix donor and acceptor molecules to increase the interface areas, so that excitons before recombination get the chance of being separated at an interface. This type of OSC is called bulk heterojunction OSC (BHJOSC). Figure 2.6 shows a very rudimentary comparison between bilayer heterojunction and bulk heterojunction structures. In this picture the black color represents acceptor layer and the white color stands for donor layer.

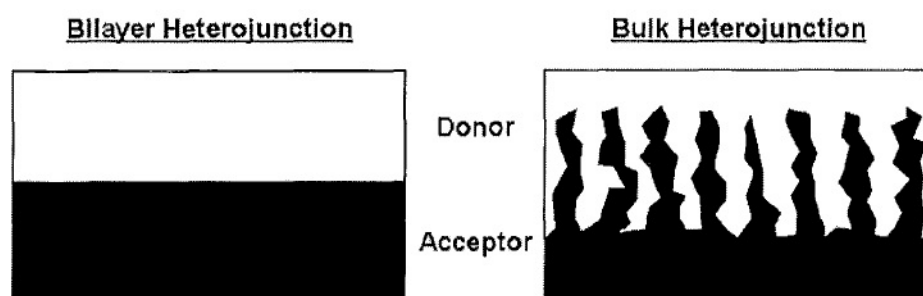


FIGURE 2.6 Difference between bulk and bilayer organic solar cell [30]

As it can be seen in the picture, in bulk heterojunction SCs these two materials are mixed together. Therefore, in bulk heterojunction SCs, the interface of the donor and acceptor layers is increased and as a result the number of excitons that get separated into electrons and holes is increased, which will lead to an increase in the ratio of generated carriers over the number of absorbed photons. This ratio is called the quantum efficiency and is one of the characteristic figures-of-merit that are used to evaluate the performance of a solar cell.

2.3.3.3 Tandem Organic Solar Cell

Tandem solar cells provide one way of increasing the overall absorption and efficiency of a solar cell. A tandem cell is essentially two (or more) solar cells stacked

directly on top of each other with a transparent electrode (recombination layer) in the middle. Light will travel through the front cell, past the transparent electrode, and into the back cell. Ideally, a tandem cell will behave like two cells in series. Therefore, the voltages produced by the two cells will add, and the current of the tandem cell will be limited by the lower current of the two cells. If the same material is used for the front and back cell, a tandem configuration can allow for an overall thicker cell to absorb more light, though the layers must be carefully designed to ensure similar photocurrent in both cells. Alternatively, materials with complementary absorption spectra can be used in the two cells to cover a broader portion of the solar spectrum, which may also reduce energy lost if photons are absorbed in materials with a band gap closer the energy of the photons. Tandem solar cell can absorb light of different wavelengths depending on the stack configuration. However, most organic, tandem solar cells to date have a lower efficiency than single-heterojunction cells with optimized geometries because of difficulties matching the photocurrent of the series-connected cells. Much research is still needed to take full advantage of the larger absorption of the solar spectrum in tandem cells and increase the overall efficiency.

2.3.4 Photocurrent Generation in Organic Solar Cell

The absorption of a photon in an inorganic solar cell can promote an electron from the valence band into the conduction band and lead to a free electron-hole pair because the binding energy between the electron and hole is small and easily overcome by the thermal energy (kT) at room temperature. The low binding energy is largely the result of the high dielectric constant of the materials and the periodicity and rigidity that create in the band structure. However, geometry relaxation effects, lower dielectric constant and electron correlation, and stronger Coulomb attraction in organic materials lead to a bound electron-hole pair, called an exciton, when light is absorbed in an organic semiconductor [31]. Excitons in organics, which typically have large binding energies on the order of 500 meV [32], must be dissociated into separate charges before they can contribute to photocurrent in an

organic cell. This dissociation can be accomplished at the interface between an appropriately chosen electron donating material (donor) and an electron accepting material (acceptor) where it is energetically favorable for the exciton to dissociate with the electron in the acceptor and the hole in the donor. Figure 2.7(a) shows a simple energy-level diagram of this situation.

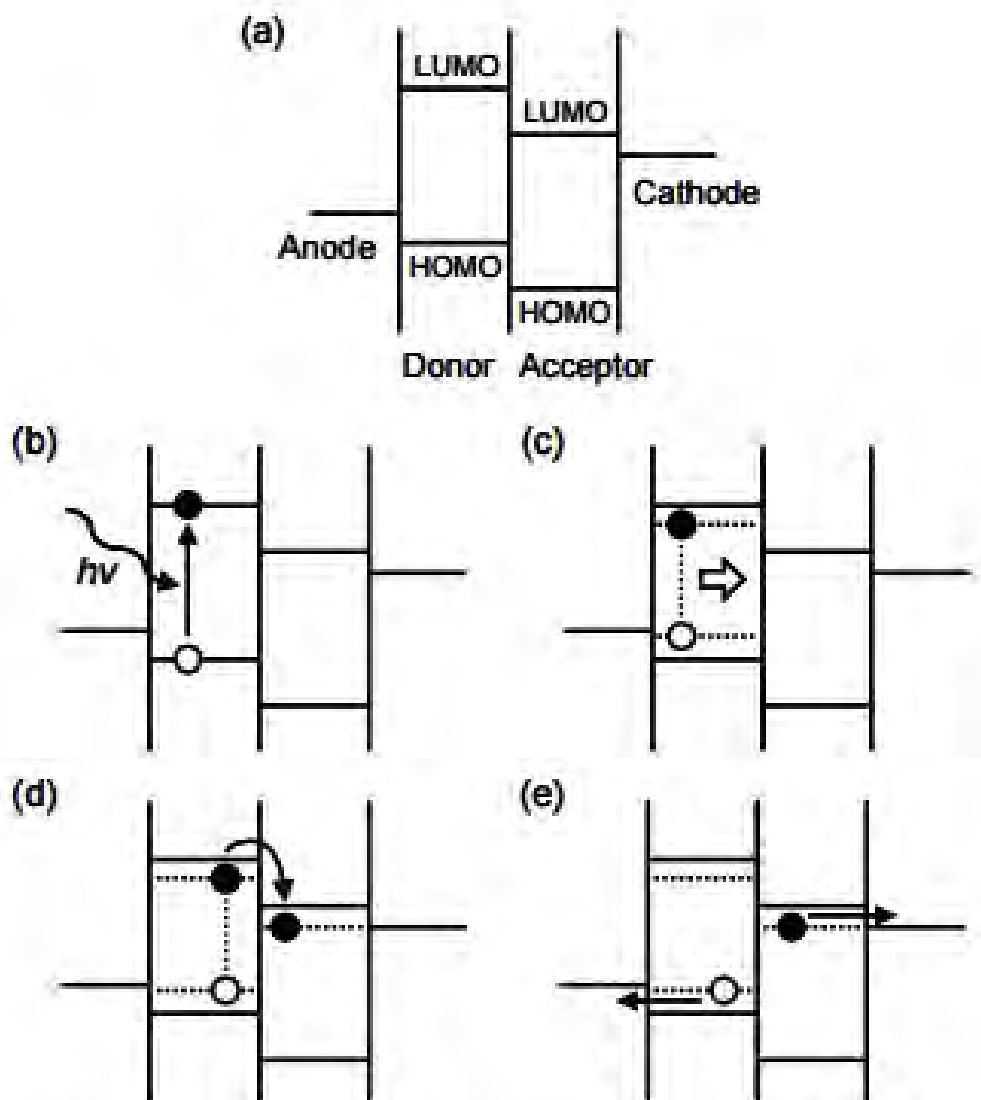


FIGURE 2.7 (a) Basic energy-level diagram for an organic solar cell. Based on the energy level diagram, overview of the photocurrent generation process: (b) light absorption to create an exciton; (c) exciton diffusion to donor / acceptor interface; (d) exciton dissociation and charge separation; and (e) charge transport and collection at the electrodes.

Photocurrent generation in an organic solar cell generally occurs in four main steps (Figure 2.7). First, the absorption of a photon excites an electron from the HOMO

of the organic material to create an exciton (Figure 2.7 b). Next, the exciton must diffuse to the donor / acceptor interface to dissociate into charge carriers (Figure 2.7 c). Because excitons have no net charge, their diffusion is generally treated as a random process based on concentration gradients without influence from electric fields [32]. However, excitons can recombine during the diffusion process before reaching the donor / acceptor interface, leading to absorbed photons that do not contribute to the current. The characteristic length an exciton travels before recombining is described by the exciton diffusion length. Exciton diffusion length affects device design because of the trade-off between light absorption and recombination as layer thickness is changed.

Excitons that do reach the donor / acceptor interface can then dissociate into electrons and holes (Figure 2.7 d). However, there is still no clear understanding of exactly how exciton dissociation occurs on a molecular level [32]. Generally, the process is described as the changing of the exciton state at the interface into a charge transfer state between an adjacent donor and acceptor followed by either recombination or dissociation into a charge-separated state. While this is the most repeated description, the entire picture is most likely more complicated, involving processes such as the interaction of additional states, the possibility of energy transfer, and the formation of different types of excitons, with the ultimate outcome determined by the relative rates of all the interactions [32]. While the full story is still the subject of much research, it appears that the energy change in going from a bound electron-hole pair to a hole in the donor (with an energy roughly estimated by the ionization potential) and an electron in the acceptor (roughly estimated by the electron affinity) is what ultimately leads to free charges.

Finally, the charges are transported through the semiconductors and collected by their respective electrodes (Figure 2.7 e). Unlike inorganic semiconductors, the charges in organic materials are generally more localized and travel through hopping processes. The different transport mechanisms lead to mobility values typically below $1 \text{ cm}^2\text{V}^{-1}\text{s}^{-1}$ that can have different dependences on temperature and electric field compared to inorganic materials. Also, choice of electrode materials and modification of the contact between the electrode and organic is

another area undergoing active research that can significantly affect the ability to extract the generated charges.

2.3.5 Challenges

While the primary factor preventing the commercial application of organic solar cells is their limited efficiency, other major challenges that must be addressed include stability and scaling. The oxygen and water present in ambient air are known to degrade the performance of most organic solar cells [33–36]. Therefore, either structures that are insensitive to air must be developed or organic cells must be encapsulated to protect them from the ambient atmosphere. For example, structures that remove the low work function electrode from the top layer of the device are being developed to help improve air stability [37, 38]. However, developing completely air stable molecules is a big challenge, so encapsulation methods are still needed.

To take full advantage of the potential for lightweight and flexible organic solar cells, encapsulation technologies that are also lightweight, thin, and flexible must be developed. The encapsulation must also be processed at temperatures that are compatible with the organic materials and flexible substrates. It has been suggested that water vapor transmission rates and oxygen transmission rates on the order of 10^{-4} to $10^{-6} gm^{-2}day^{-1}$ and 10^{-3} to $10^{-5} cm^3m^{-2}day^{-1}atm^{-1}$, respectively, are necessary to maintain long shelf lifetime in organic solar cells [39]. Currently, the most promising candidates for encapsulation are alternating thin films of inorganic and organic materials. The inorganic layers serve as the primary barrier to water and oxygen, while the organic layers serve to interrupt defects that would propagate through a single, continuous inorganic film [40]. Thin-film encapsulation layers on top of organic solar cells are now starting to be demonstrated with improved performance [35, 36, 41].

The issues that arise when scaling up to large-area devices must also be addressed. Presently, many of the high-efficiency devices that are reported in the literature

have active areas of 1 cm^2 or less. The large-area devices that have been reported are usually modules consisting of several smaller cells with overall efficiencies less than half that of a single, optimized, small-area cell [39]. The main problem with increasing cell size stems from the use of a transparent electrode with a relatively high sheet resistance. The low conductivity of the transparent electrodes results in low fill factor and short-circuit current in large-area devices; therefore, overall efficiency is expected to decrease as device area is increased. Strategies must be developed to deal with these losses as area increases. While significant progress has been made in the field of organic solar cells, it is clear that many challenges still remain.

2.4 Different Parameters of Solar Cell

For solar cell characteristics, current-voltage curve is obtained first. From that curve different parameters are obtained. Each of this parameter will be described below:

2.4.1 Open Circuit Voltage (V_{oc})

The open circuit voltage is the voltage across the solar cell when $J=0$, which is the same as device being open circuited. Because $J=0$, and power is the product of current and voltage no power is actually produced at this voltage. However, the V_{oc} marks the boundary for voltages at which power can be produced. The open-circuit voltage can also be thought of as the point at which the photocurrent generation and dark current processes compensated one another.

2.4.2 Short Circuit Current Density (J_{sc})

Similar to V_{oc} the short circuit current density J_{sc} is the current density when $V = 0$ which is the same conditions as the two electrodes of the cell being short

circuited together. Again, there is no power produced at this point, but the J_{sc} will mark the onset of power generation. In ideal devices, the J_{sc} will be same as photocurrent density. However, it will be seen later that several effects can lower the J_{sc} from this ideal value. Although J_{sc} is technically a negative number with the conventions used here, discussions of different J_{sc} values will focus primarily on the magnitude of the value and treat it as a positive number.

2.4.3 Fill Factor (FF)

While V_{oc} and J_{sc} mark the boundaries of power production in a solar cell, the maximum power density produced P_{max} occurs at the voltage V_{max} and the current density J_{max} where the product of J and V is at a minimum. Because of the diode behaviour and additional resistance and recombination losses, $|J_{max}|$ and V_{max} are always less than $|J_{sc}|$ and V_{oc} respectively. The fill factor is defined as

$$FF = \frac{J_{max}V_{max}}{J_{sc}V_{oc}} \quad (2.1)$$

FF is an indication of how close J_{max} and V_{max} come to the boundaries of power production of J_{sc} and V_{oc} and also indication of the sharpness of the bend in the exponential J-V curve. Since higher FF means higher maximum power, high FF is desired. Now it is evident from the fact that J_{max} and V_{max} is always less than J_{sc} and V_{oc} , FF is always less than one.

2.4.4 Power Conversion Efficiency

The most discussed performance parameter of a solar cell is the power conversion efficiency η and is defined as the percentage of incident irradiance P_{in} that is converted into output power. Because of the point where the cell operates on the J-V curve changes depending on the load, the output power depends on the load. For consistency, the maximum power is used for calculating efficiency. It can be defined as,

$$\eta = \frac{J_{max}V_{max}}{P_{in}} * 100\% = \frac{J_{sc}V_{oc}FF}{P_{in}} * 100\% \quad (2.2)$$

This form clearly shows that FF, J_{sc} and V_{oc} all have effects on η . Furthermore, the area used to calculate J can affect η and should include inactive areas that are integral to the solar cell. This efficiency is also dependent of the solar irradiation spectrum.

Power conversion efficiency is important since it determines how effectively the space occupied by a solar cell is being used and how much area must be covered with solar cells to produce a given amount of power. Since larger areas require more resources to cover with solar cells, higher is often desirable. However, there are tradeoffs between η and cost for each solar cell technology that must be balanced.

Power conversion efficiency is also very dependent on the power and spectrum of the light source since solar cells do not absorb and convert photons to electrons at all wavelengths with the same efficiency. A standard spectrum must be chosen for the calculation of η in order to compare among various solar cells. Although the spectrum of the sunlight at the earths surface varies with location, cloud coverage, and other factors, the AM 1.5 G spectrum in Figure 2.8 is the most commonly used standard spectrum for measuring and comparing the performance of photovoltaics that are intended for outdoor use.

2.5 Different Modeling Scheme for Bulk Hetero-junction Organic Solar Cell

Modeling of a device is necessary to understand device performance, find out the effect of different parameters which are too expensive or very much difficult to measure and propose new devices with increased performance. To support the experimental data, it is necessary to get a model that can describe obtained data. As, organic solar cell is being researched extensively by the researchers to get a low

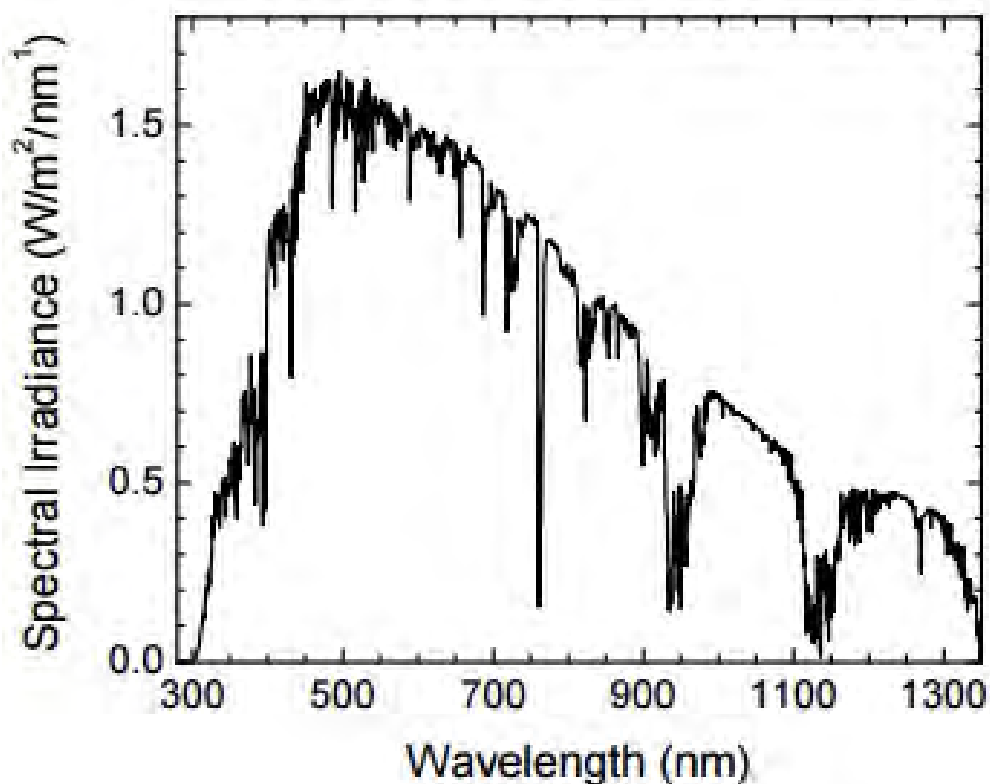


FIGURE 2.8 Spectral irradiance of AM1.5G solar spectrum up to 1350 nm [42]

cost and flexible solar cell, various models are proposed by numerous researcher. A couple of widely used models are described below.

2.5.1 Koster Model

Koster Model is described in [43–45]. The model calculates the photon absorption using transfer matrix theory. By calculating the absorbed photon rate, exciton generation rate is calculated. It is assumed that the carrier mobility is constant for all electric field. At first, a potential, electron density and hole density is assumed. Exciton diffusion is considered. Recombination of the charge carriers are modeled by reduced bimolecular recombination due to the fact that only slowest carrier determines the recombination rate in bulk heterojunction organic solar cell. After assuming, voltage, electron density and hole density Poisson equation is used. Now if the change in potential is greater than the convergence parameter then loop is continued. If the convergence is achieved then charge transport equation

is used and new electron and hole density is calculated. Current is modeled by drift-diffusion term. Now if the change in electron and hole density is less than convergence parameter, total current density is calculated otherwise loop starts again. Flow chart of this model is given in Figure 2.9

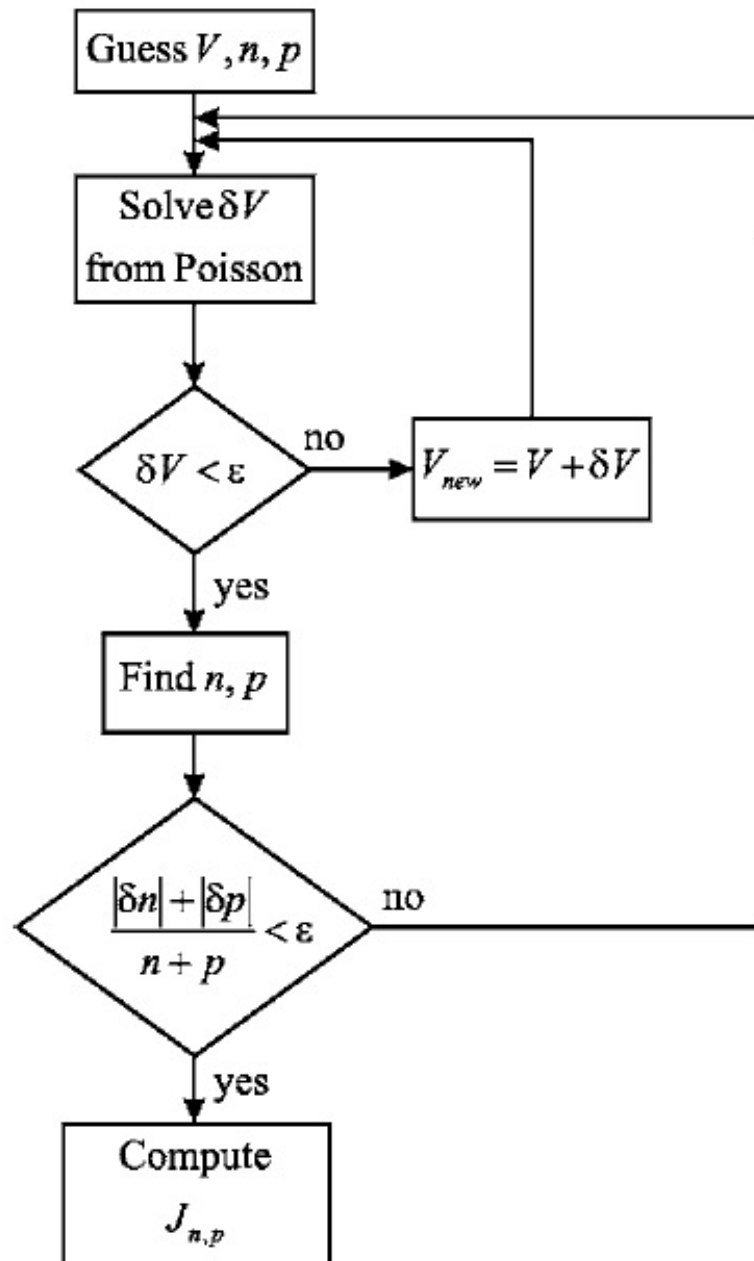


FIGURE 2.9 Koster model for calculation of current-voltage characteristics of organic solar cell with constant carrier mobility [43]

2.5.2 Analytical Model

Analytical models deal with different equation and assumptions [46]. It varies from author to author. If anyone wants to develop an analytical model he or she has to assume some phenomena and modify equations according to his assumptions. If the modeled data is consistent with the experimental results then the model is valid.

2.5.3 Morphological Model

Bulk Heterojunction device performance depends on annealing and morphology [47]. As when annealing is done then the solvent mixes and morphology changes. With the change in morphology, mobility and other parameter of the device changes. So researchers model the morphology first using dynamic Monte Carlo method and then model the device performance [17, 48].

Chapter 3

Results and Discussions

3.1 Performance Analysis of Bilayer Organic Solar Cell

Bilayer organic solar cell is considered as Planar Heterojunction Device [23]. Both bilayer and bulk heterojunction solar cell fabrication are reported in the literature [49–56]. So at first, performance of bilayer organic solar cell will be analysed in this chapter. For the analysis of the device P3HT is selected as donor layer, PCBM is selected as acceptor layer, Indium Tin Oxide (ITO) is used as anode material and Aluminium (Al) is used as cathode material. Now organic photovoltaic operation in bilayer solar cell can be divided into four steps as discussed in Chapter 2. Each step is modeled by the following equations. All the simulation is done by the OPV tool available online [47].

- **Photon Absorption:** Photon absorption process occurs when light is absorbed in the photoactive layer of the organic solar cell. Photon absorption in different layer of the device is calculated using transfer matrix formalism considering AM 1.5G solar irradiance. The absorption profile depends on refractive index and thickness of different layer.

- **Exciton Diffusion:** Absorbed photon creates a tightly bound electron-hole pair namely exciton in the organic material. As exciton has to travel Donor-Acceptor (DA) interface to create free charge carriers, travelling of excitons are modeled by the following exciton diffusion equation in this tool.

$$D_{ex}\nabla^2 n_{ex} = G_{ex}(r) - R_{ex}(n_{ex}) \quad (3.1)$$

where,

G_{ex} = Exciton generation rate

R_{ex} = Exciton recombination rate

D_{ex} = Exciton diffusion coefficient

τ_{ex} = Exciton life time

Now the exciton diffusion can be defined as $L_{ex} = \sqrt{D_{ex}\tau_{ex}}$ and it is used as an input parameter for the simulation.

- **Charge Carrier Generation:** Excitons that arrive at the DA interface will be dissociated into free charge carriers. In the tool exciton dissociation probability is considered as high so that it is assumed that exciton concentration at the DA interface is zero. Only the excitons generated within a distance of exciton diffusion length will contribute to the photocurrent as other excitons will be decayed.
- **Charge Transport:** After the dissociation of excitons holes travel through the donor layer and electrons travel through the acceptor layer. Both charge carrier is driven through by the electric field in the active layer originated from the work function difference of the electrodes. Charge transport is modeled by the following drift-diffusion transport equation in this tool.

$$J_n = q\mu_n n(x) E(x) + qD_n \nabla n(x) \quad (3.2)$$

$$J_p = q\mu_p p(x) E(x) - qD_p \nabla p(x) \quad (3.3)$$

where,

μ_n = Electron mobility

μ_p = Hole mobility

D_p = Hole diffusion coefficient

D_n = Electron diffusion coefficient

$n(x)$ = Electron concentration

$p(x)$ = Hole concentration

$E(x)$ = Electric field

Electric field is calculated by the self consistent simulation of Poisson equation and transport equations.

3.1.1 Effect of Acceptor Layer Thickness on Device Performance

Using the simulation tool, bilayer solar cell performance with a variation of active layer thickness is analysed. Exciton diffusion length of P3HT organic layer can vary from 3nm to 7 nm [57]. In this simulation it is assumed that donor exciton diffusion length is 5 nm. Typical values of electron and hole mobility $0.001 \text{ cm}^2/V.s$ and $0.0001 \text{ cm}^2/V.s$ are used respectively in this simulation.

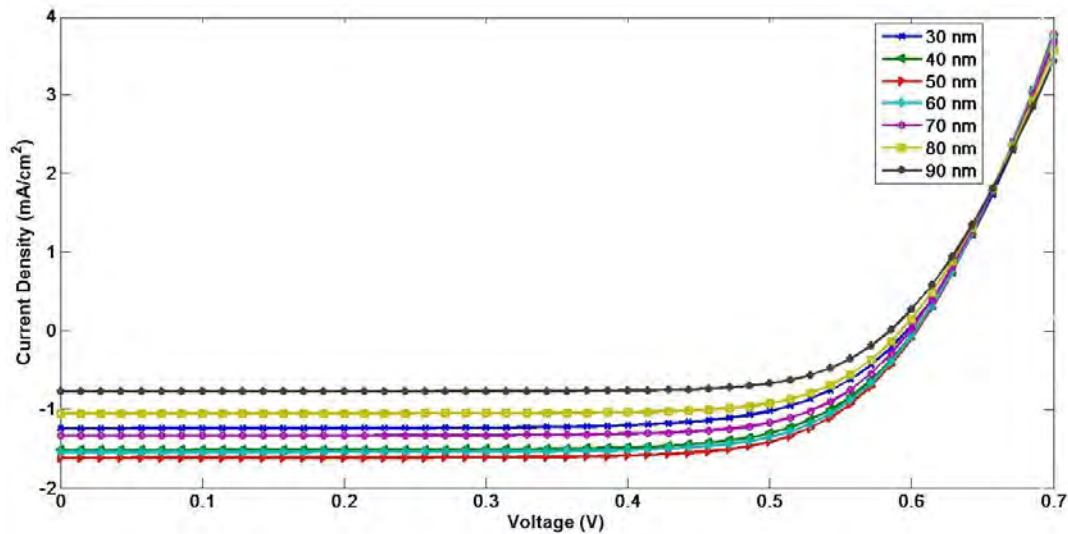


FIGURE 3.1 Effect of Acceptor Layer Thickness on Current-Voltage Characteristics.

From the Figure 3.1 it is evident that, upto 50 nm of acceptor layer the short circuit current increases and open circuit voltage remains same. But after that short circuit current decreases with the increase of acceptor layer thickness. It can be attributed to the fact that at the beginning from 30 nm to 50 nm increasing acceptor layer thickness results more photon absorption and hence increases current. But after that most of the charges recombine so that current decreases. Efficiency also follows the same pattern as current as shown in Figure 3.2.

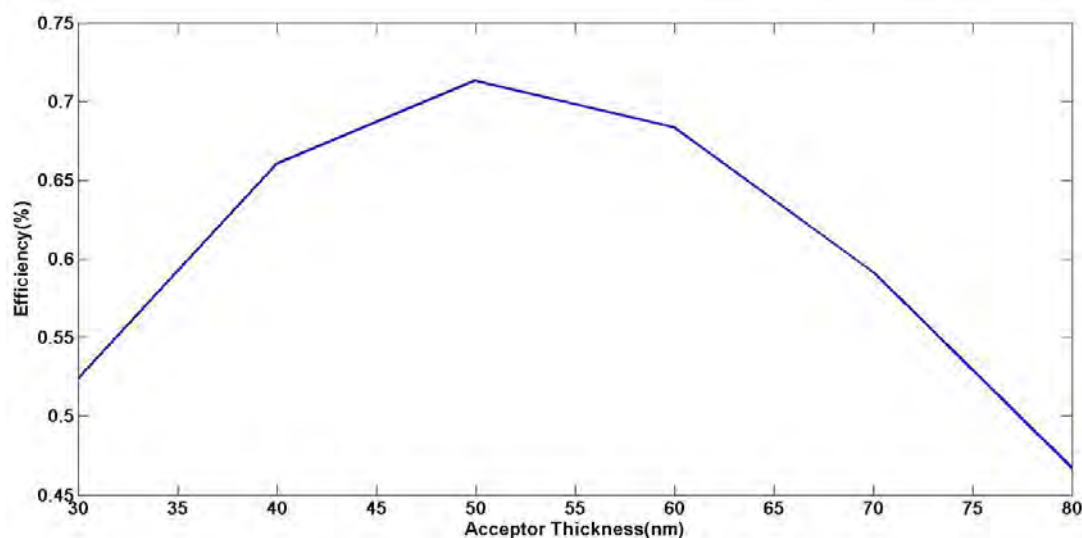


FIGURE 3.2 Effect of Acceptor Layer Thickness on Solar Cell Efficiency.

3.1.2 Effect of Donor Layer Thickness on Device Performance

As bilayer organic solar cell has both donor and acceptor layer, so thickness of each layer has an impact on the performance. In order to find out the effect of donor layer thickness all parameters are kept as same as previous section 3.1.1. Acceptor layer thickness is kept at 50 nm as this thickness gives the maximum efficiency and current. Now, donor layer thickness is varied from 30 nm to 100 nm and obtained current-voltage characteristics is shown in the following figure.

From Figure 3.3, it can be seen that increasing donor layer thickness decreases current and open circuit voltage remains same as the difference between work

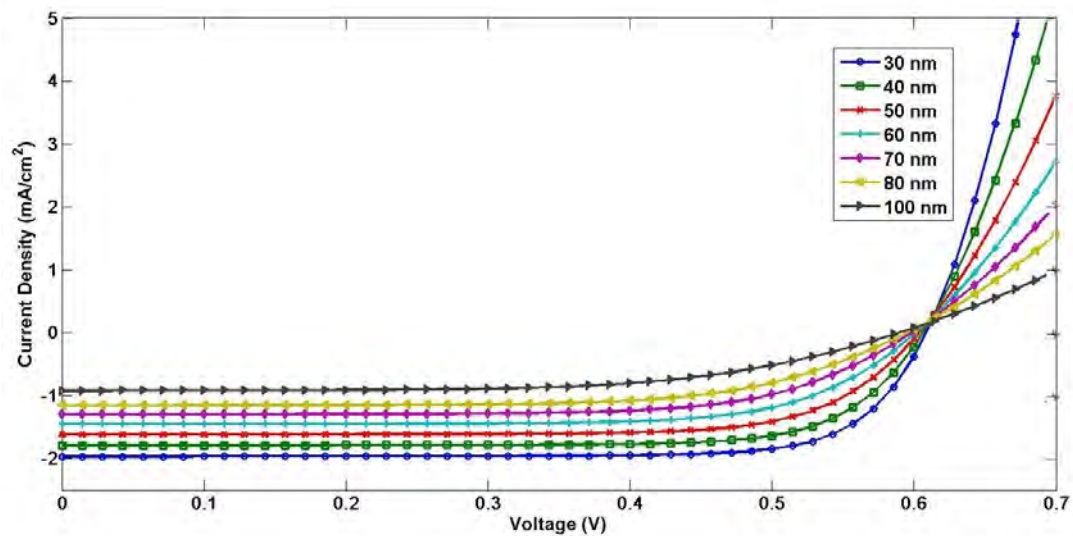


FIGURE 3.3 Effect of donor layer thickness on current-voltage characteristics of bilayer organic solar cell

function of the two electrode does not change with the variation of donor layer thickness. As, exciton diffusion length in P3HT is very small, so if the donor layer thickness is increased very much then most of the excitons cannot reach to the donor-acceptor(DA) interface. Though photon will be absorbed more with the increase in donor layer thickness but as most excitons are decayed instead of dissociation into free charge carriers current decreases with the increase in donor layer thickness.

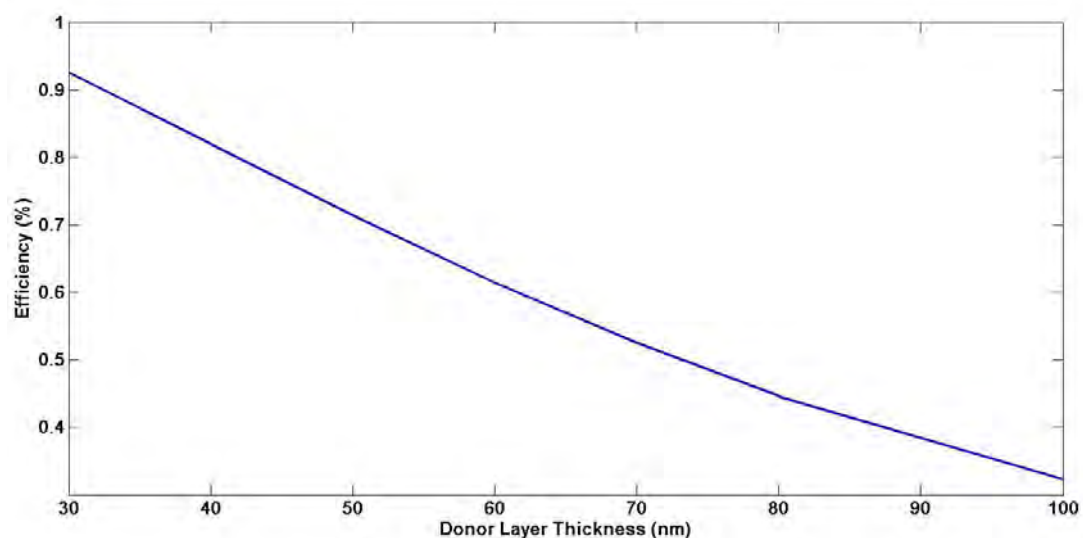


FIGURE 3.4 Effect of Donor Layer Thickness on efficiency of bilayer organic solar cell

From Figure 3.4, it is seen that efficiency of the bilayer organic solar cell decreases with the increase in donor layer thickness. The loss in current with the increase of thickness can be attributed as the reason of reduced efficiency.

3.1.3 Effect of Electron Mobility on Device Performance

Variation of electron mobility in acceptor can change the device performance. Higher mobility means electrons move faster in the acceptor material and electron can easily transport from Donor Acceptor interface to electrode. So at higher mobility device performance should be better which is evident from the obtained J-V characteristics shown in the following figure. In this simulations all parameters are as same as section 3.1.1 except electron mobility is varied and acceptor layer thickness is kept at 50nm.

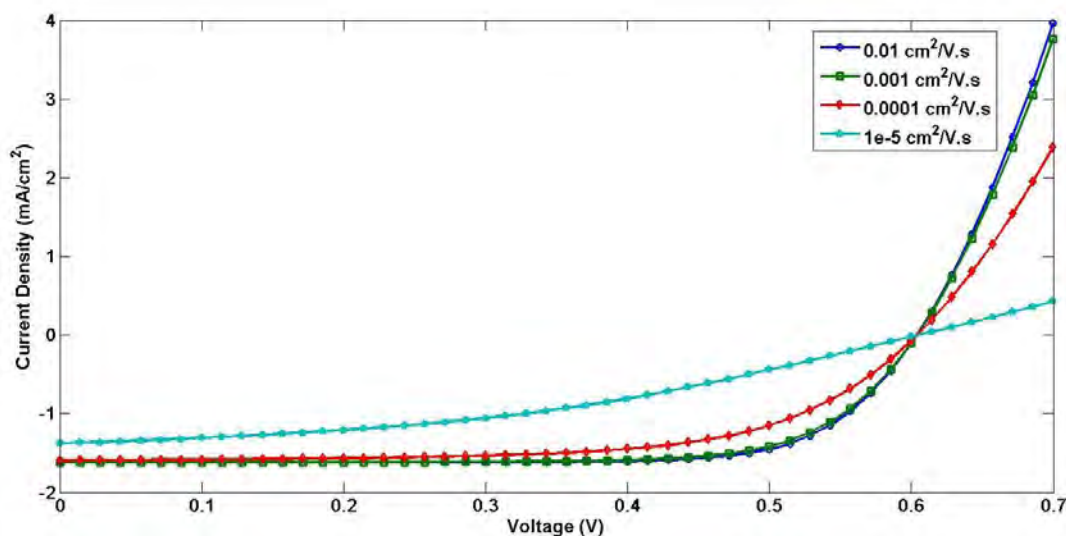


FIGURE 3.5 Effect of Electron Mobility on Current-Voltage Characteristics

From Figure 3.5, it is seen that at higher mobility performance is almost constant but when the mobility is reduced then the performance of the device falls in a destructive way which is expected. From the efficiency curve in Figure 3.6 the claim can be validated.

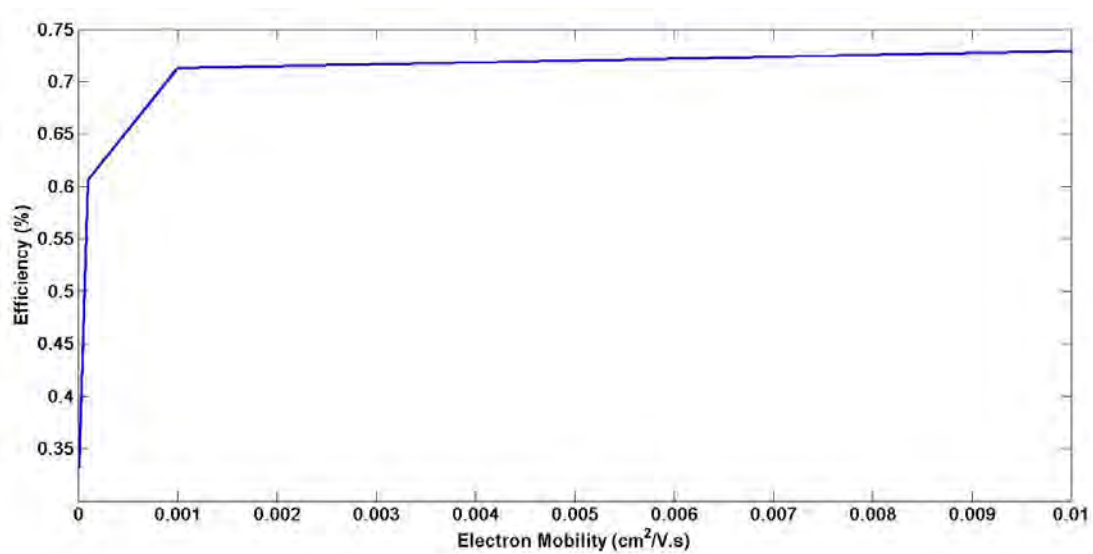


FIGURE 3.6 Effect of Electron Mobility on efficiency of bilayer organic solar cell

3.1.4 Discussion

From the result of this section, it can be inferred that efficiency and short circuit current of bilayer organic solar cell is very low. It can be attributed to the fact that excitons created by the absorbing photon decays to ground state before reaching to the donor acceptor interface. Moreover small exciton diffusion length also emphasises the outcome. So, a device structure where donor-acceptor interface will be more readily available is sought for better efficiency. Hence, bulk heterojunction solar cell structure comes. In the next section, modeling scheme of bulk heterojunction solar cell considering electric field mobility is discussed.

3.2 Modeling of Bulk Heterojunction Organic Solar Cell

The goal of modeling organic solar cells is to find new device designs, to enhance the understanding of the power generation in these devices and to improve the performance of these devices based on the understanding. Modeling provides an opportunity to examine properties that are out of reach or too expensive to measure. On the other hand, modeling is much faster and makes it possible to

study numerous device structures and configurations in a very short period of time, which can provide valuable information. These abilities are beyond what an experiment can do. By taking the device as a light-in current-out device the performance of solar cells can be divided into the following processes:

1. In-coupling of the photons
2. Absorption of the photons
3. Formation of the excitons from absorbing photons
4. Diffusion of excitons into Donor-Acceptor interface
5. Dissociation of excitons
6. Transport of charge carriers
7. Collection of the charges at the electrode

Now as seen in Figure 3.2 efficiency of bilayer organic solar cell is very low, Bulk heterojunction (BHJ) solar cell where acceptor and donor and acceptor are mixed in a solution used as active layer and cast into a thin film sandwiched between two electrode are introduced [58–62]. All of these above mentioned processes are incorporated in this modeling considering electric field dependent carrier mobility. As it is known that, if the active layer thickness is varied then the electric field in the active layer will be changed. So the effect of this change in electric field result in different carrier mobility which needs to be incorporated in the modeling. Now the first three points will be discussed in Optical Modeling section and the last four will be discussed in Electrical Modeling Section.

3.2.1 Optical Modeling of Bulk Heterojunction Organic Solar Cell

Optical modeling of bulk organic solar cell deals with the photon absorption in the active layer and these photons transfer their energy to create excitons in the

device. In this model, light is assumed to be injected at a normal angle to the device. The injected light is assumed to be planar waves. As mobility of organic materials is low and there is requirement of strong electric field for the dissociation of the exciton, active layer needs to be thin. So, interference effect is needed to be considered to calculate total absorbed photon.

Since excitons generated in Organic Photovoltaic (OPV) devices can diffuse to the Donor-Acceptor (DA) interface and dissociate, the location of the exciton generation has impact on the device performance. Therefore, in order to correctly model the organic solar cell devices, we need to calculate the photon absorption at each position. In other words, we need to calculate the photon absorption at each monolayer after dividing the device into different discrete monolayers.

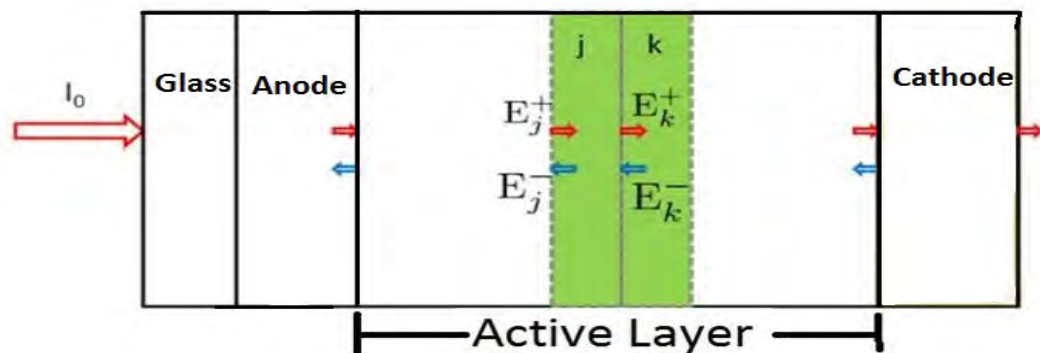


FIGURE 3.7 Diagram of the photon absorption in typical BHJ devices. E_j^+ and E_j^- are the components of the optical electric field propagating in the positive and negative directions in the j^{th} monolayer, E_k^+ and E_k^- are the corresponding parameters for the adjacent k^{th} monolayer.

The absorption in BHJ devices is modeled by the transfer matrix theory [63, 64]. Figure 3.7 shows the diagram of the photon absorption in OPV devices. Because of the reflectance of the back cathode, the optical electric field at any position can be decomposed into two components; one component propagating in the positive direction and the other in the negative direction. Given that E_j^+ and E_j^- are the components of the optical electric field propagating in the positive and negative directions in the j^{th} monolayer respectively, and E_k^+ and E_k^- are the corresponding parameters for the adjacent k^{th} monolayer.

In the transfer matrix method solar cell is modeled by two types of matrices and they are:

- **Interface Matrix:** It models the phenomena of transportation and reflection of incoming beam of light at the interface of two adjoining layers. The matrix can be defined as:

$$I_{jk} = \frac{1}{t_{jk}} \begin{bmatrix} 1 & r_{jk} \\ r_{jk} & 1 \end{bmatrix} \quad (3.4)$$

where r_{jk} and t_{jk} are the Fresnel complex reflection and transmission coefficients at interface jk . As, it is assumed that light is injected normally, Fresnel reflection and transmission coefficients are defined by,

$$r_{jk} = \frac{\widetilde{n}_j - \widetilde{n}_k}{\widetilde{n}_j + \widetilde{n}_k} \quad (3.5)$$

$$t_{jk} = \frac{2\widetilde{n}_j}{\widetilde{n}_j + \widetilde{n}_k} \quad (3.6)$$

where \widetilde{n}_j and \widetilde{n}_k are the complex refractive index in the j^{th} monolayer and the k^{th} monolayer, respectively. Absorption strength depends on the imaginary part of the refractive index, namely extinction coefficient.

- **Layer Matrix:** It models the effect of each layer's material on transporting beam of light. It describes the propagation through that layer. For layer j , layer matrix is given by,

$$L_j = \begin{bmatrix} e^{-i* \frac{2\pi\widetilde{n}_j d_j}{\lambda}} & 0 \\ 0 & e^{i* \frac{2\pi\widetilde{n}_j d_j}{\lambda}} \end{bmatrix} \quad (3.7)$$

where, d_j is the thickness of monolayer.

Now, by using this interface matrix from Equation 3.4 and layer matrix from Equation 3.7, relation between the two adjacent layer's electric field can be calculated. This relation can be expressed as,

$$\begin{bmatrix} E_j^+ \\ E_j^- \end{bmatrix} = I_{jk} L_j \begin{bmatrix} E_k^+ \\ E_k^- \end{bmatrix} \quad (3.8)$$

After calculating all the transfer matrices in the devices and multiplying them together, we can achieve a final matrix. The final matrix connects the optical electric fields of the 0^{th} monolayer (layer in front of the BHJ device) and the $(N + 1)^{th}$ monolayer (layer at the back of the BHJ device) and it can be defined as,

$$\begin{bmatrix} E_0^+ \\ E_0^- \end{bmatrix} = S \begin{bmatrix} E_{N+1}^+ \\ E_{N+1}^- \end{bmatrix} \quad (3.9)$$

where, S is scattering matrix and it can be written as,

$$S = \begin{bmatrix} S_{11} & S_{12} \\ S_{21} & S_{22} \end{bmatrix} = \left(\prod_{v=1}^N I_{(v-1)v} L_v \right) I_{N(N+1)} \quad (3.10)$$

Now, E_0^+ is related to the incident light, and that $E_{N+1}^- = 0$ as no light come back after it get out of the device, we can figure out the other two variables E_0^- and E_{N+1}^+ by solving the matrix equation. For the total layered structure the complex transmission and reflection coefficients can be expressed as

$$r = \frac{E_0^-}{E_0^+} = \frac{S_{21}}{S_{11}} \quad (3.11)$$

$$t = \frac{E_{N+1}^+}{E_0^+} = \frac{1}{S_{11}} \quad (3.12)$$

With the optical electric field in 0^{th} monolayer, optical electric field in other monolayers can be calculated by using transfer matrix iteratively. Reflection of the glass substrate is taken into account to calculate the initial optical electric field at the glass-ITO interface by the following equation [65].

$$|E_{0g}|^2 = \frac{1 - R^*}{\eta_g(1 - RR^*)} |E_0|^2 \quad (3.13)$$

where R^* represents the reflectance of air/glass interface, R the reflectance for the stack structure, η_g the refraction coefficient of glass and $|E_0|^2$ (modulus squared of the optical electric field) the initial intensity of optical electric field when light arrives at air/glass interface.

After calculating the optical electric field at each monolayer average absorbed power can be calculated for each wavelength. The average absorbed light power is given by,

$$Q_j = \frac{4\pi c \epsilon_0 k_j n_j}{2\lambda} |E_j^+ + E_j^-|^2 \quad (3.14)$$

where Q_j is the absorption rate at j^{th} monolayer, n_j is real part of refractive index, k_j is imaginary part of refractive index, c is velocity of light and ϵ_0 is vacuum dielectric constant. Now total absorbed photon is calculated considering AM 1.5G irradiance with integrated intensity 100 mW/cm^2 using Equation 3.15.

$$N = \int_{\lambda=300nm}^{900nm} Q(\lambda) \frac{\lambda}{hc} d\lambda \quad (3.15)$$

Each photon then transfer their energy and become excitons after that. So at the end of the optical modeling, total generation rate of exciton is obtained.

3.2.2 Electrical Modeling of Bulk Heterojunction Organic Solar Cell

The electrical model considers the generation, recombination, drift, diffusion, and collection process of the electron and hole in the active BHJ layer. At first exciton

dissociates in the DA interface. After that free charge carrier generation, recombination and transport of charges occur. All of these processes will be incorporated in the modeling considering electric field dependent carrier mobility.

3.2.2.1 Exciton Dissociation in BHJ Device

Excitons, rather than free charge carriers, are formed after the photon absorption in OPV devices because of the low dielectric constant and strong exciton binding energy. Excitons can diffuse to the donor acceptor (DA) interface and dissociate efficiently. For bulk heterojunction devices it is assumed that DA interfaces are uniformly distributed all over the active layer and exciton dissociate immediately after its creation. So, diffusion of exciton is ignored in this model. To calculate the exciton dissociation, we assume that the charge transfer (CT) process takes place immediately after excitons arrive at the DA interface [43–45]. The new CT state can either dissociate into free charge carriers with a field dependent rate k_d and or decay to the ground state with a constant rate k_f . The dissociation rate k_d of CT state is calculated through the Braun-Onsager model [43, 48, 66]. The equation is given by,

$$k_d = \frac{e}{4\pi a^3} * \frac{e * (\mu_p + \mu_n)}{\epsilon_r \epsilon_0} * \exp\left(\frac{-e}{4\pi \epsilon_r \epsilon_0 a k T}\right) * \left(1 + b + \frac{b^2}{3} + \frac{b^3}{18} + \dots\right) \quad (3.16)$$

where,

$$b = \frac{e^3 E}{8\pi \epsilon_r \epsilon_0 k^2 T^2} \quad (3.17)$$

E = Electric Field

μ_n = Electron mobility

μ_p = Hole mobility

a = Charge carrier initial separation distance in the CT state

ϵ_r = Relative dielectric constant

e = Electron charge

k = Boltzman Constant

T = Temperature

The model was originated by Onsager for analysis of geminate recombination of an ion pair in an isotropic medium [45, 66]. The model has been used in [43] for calculating the photogeneration of charges in bulk heterojunction OPV cells. The two key parameters that control the dissociation efficiency are a and k_f . A large separation distance can help to dissociate the CT state while a large k_f can make the CT state more likely to decay rather than dissociate.

3.2.2.2 Charge Carrier Generation, Transport and Recombination

The BHJ layer is a mixture of donors and acceptors exhibiting a complex morphology. In the following figure P3HT:PCBM BHJ solar cell structure and energy level is shown. The photogenerated excitons in the donor and the acceptor dissociate into free charge carriers at the interface. The photogenerated electrons and holes are transported in the acceptor and donor phases, respectively. In the effective medium model the BHJ layer is considered a homogeneous semiconductor [62, 67–69]. The energy difference between the LUMO of the acceptor(PCBM) and the HOMO of the donor (P3HT) is called as effective bandgap E_g .

Due to the amorphous structure of organic materials, charge carriers mainly move by hopping between molecules. The energy and position disorder impedes the transport and cause a low mobility for organic materials. As a result of the disordered structure, most organic materials have electric field dependent mobility. The electric field dependence of mobility can be described by the Poole-Frenkel equation [48, 70, 71] as follows

$$\mu(E) = \mu_0 \exp(\gamma\sqrt{E}) \quad (3.18)$$

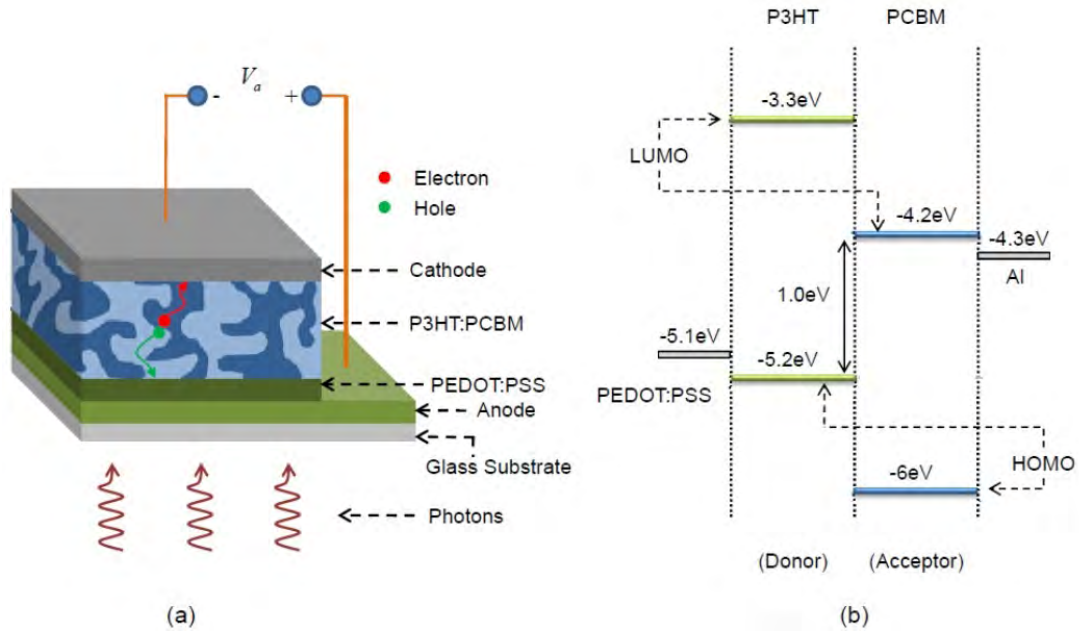


FIGURE 3.8 (a) Configuration of P3HT:PCBM based BHJ OSC and (b) Schematic energy potential diagram of the considered cell (before the materials are brought into contact). The picture is adapted from [46]

where E is the electric field, $\mu(E)$ is the charge carrier mobility under electric field E , μ_0 is the mobility under zero electric field, and γ is the Poole-Frenkel field dependence factor. Since μ_0 and γ are both constant, the mobility of the organic material under any given electric field can be calculated through the above equation

To correctly model the charge carrier transport in organic semiconductor devices, it is needed to calculate the electric field and charge carrier density distributions across the whole device. The device is treated as one-dimensional cells along the direction normal to the electrode surfaces. Therefore, the one-dimensional Poisson equation describes the electric field distribution across the organic layer, and the applied voltage across the device provides the necessary boundary condition [43, 62, 63]. The electric field in the device is calculated by the following equations.

$$\frac{\partial E}{\partial x} = \frac{e(p-n)}{\epsilon_r \epsilon_0} \quad (3.19)$$

$$V(L) - V(0) = \frac{E_g}{e} - V_a \quad (3.20)$$

where V_a is applied voltage, p is hole concentration, n is electron concentration and E is electric field. Charge carriers transport through drift diffusion equation and diffusion constant is assumed to follow Einstein relation [72, 73]. So the equation of current becomes,

$$J_n = J_{ndrift} + J_{ndiffusion} = qD_n \frac{\partial n}{\partial x} + \mu_n qnE \quad (3.21)$$

$$J_p = J_{pdrift} + J_{pdiffusion} = -qD_p \frac{\partial p}{\partial x} + \mu_p qpE \quad (3.22)$$

$$\frac{D_n}{\mu_n} = \frac{D_p}{\mu_p} = \frac{kT}{e} \quad (3.23)$$

Electrons and holes recombine with each other if they are both present in the device and are close to each other. The bulk recombination rate of free electrons and holes is calculated in accordance with Langevins theory [74].

$$R = \frac{e}{\epsilon_r \epsilon_0} (\mu_n + \mu_p) * (np - n_i^2) \quad (3.24)$$

Modified recombination equation is needed to be used in bulk heterojunction device as recombination only occur at the interface. So the slowest carrier determines the recombination rate of the device and modified equation will be

$$R = \frac{e}{\epsilon_r \epsilon_0} \min(\mu_n, \mu_p) * (np - n_i^2) \quad (3.25)$$

The drift and diffusion currents move the charge carriers in the device, while the recombination reduces the charge carrier density. Combining all of them together,

it can be calculated the change of charge carrier density over time through the continuity equation below:

$$\frac{\partial n}{\partial t} = \frac{1}{e} \frac{dJ_n}{dx} + G - R \quad (3.26)$$

$$\frac{\partial p}{\partial t} = -\frac{1}{e} \frac{dJ_p}{dx} + G - R \quad (3.27)$$

where G is the generation rate of the free charge carrier. Now as generation rate is dependent on exciton generation and dissociation rate. So exciton dissociation and decay rate are needed to be incorporated to calculate the generation rate. Again when the electron and hole recombine exciton is generated. So this is also needed to be incorporated here. Modified equation will be,

$$\frac{dX}{dt} = G + R - k_f X - k_d X \quad (3.28)$$

and continuity equation becomes

$$\frac{\partial n}{\partial t} = \frac{1}{e} \frac{dJ_n}{dx} - R + k_d X \quad (3.29)$$

$$\frac{\partial p}{\partial t} = -\frac{1}{e} \frac{dJ_p}{dx} + k_d X - R \quad (3.30)$$

where k_d is calculated using Equation 3.16.

Charge carriers in the device determine the electric field distribution, and the electric field will modify the charge carrier distribution. The interplay between the charge carriers and the electric field is the key issue in organic semiconductor devices, while the field dependent mobility further complicates the problem. In the model, the change of the exciton density and charge carrier density at each position

over time will be calculated. The model stops at the equilibrium state where the exciton density and charge carrier density at each position remain constant.

3.2.2.3 Outline of Modeling

In the above subsections each component of the model is described. Now the steps of the model are described in this section. At first, photon absorption in the active layer is calculated using optical modeling. An applied voltage is given on the active layer of the device. the corresponding charge carrier density is calculated after that. Electric field is calculated using the given voltage on the active layer. After that mobility of the charge carrier is calculated using Equation 3.18. After calculating mobility, continuity equation is used in order to calculate electron density and hole density. Now when exciton dissociates it creates electron and hole and when charge carriers recombine they create excitons. These phenomena is achieved by Equation 3.28. Equation 3.29 and 3.30 are used to calculate the new electron and hole density. Now if the change in exciton density, electron density and hole density in between iterations is less than the convergence parameter then current density is calculated, otherwise the loop is again started and it runs until the value is converged. The flow chart of the model is depicted in Figure 3.9.

3.3 Results of Optical Modeling

By doing optical modeling absorption rate of the photons and hence the generation rate of excitons can be determined for bulk heterojunction solar cell. Amount of light absorbed and photon generation is important to calculate the total current. For bulk heterojunction organic solar cell it is assumed that donor-acceptor interface is uniformly distributed. So the amount of absorbed photon is equal to the exciton generation rate at each layer of the device. Absorption of each layer under different wavelength can also be determined by this modeling.

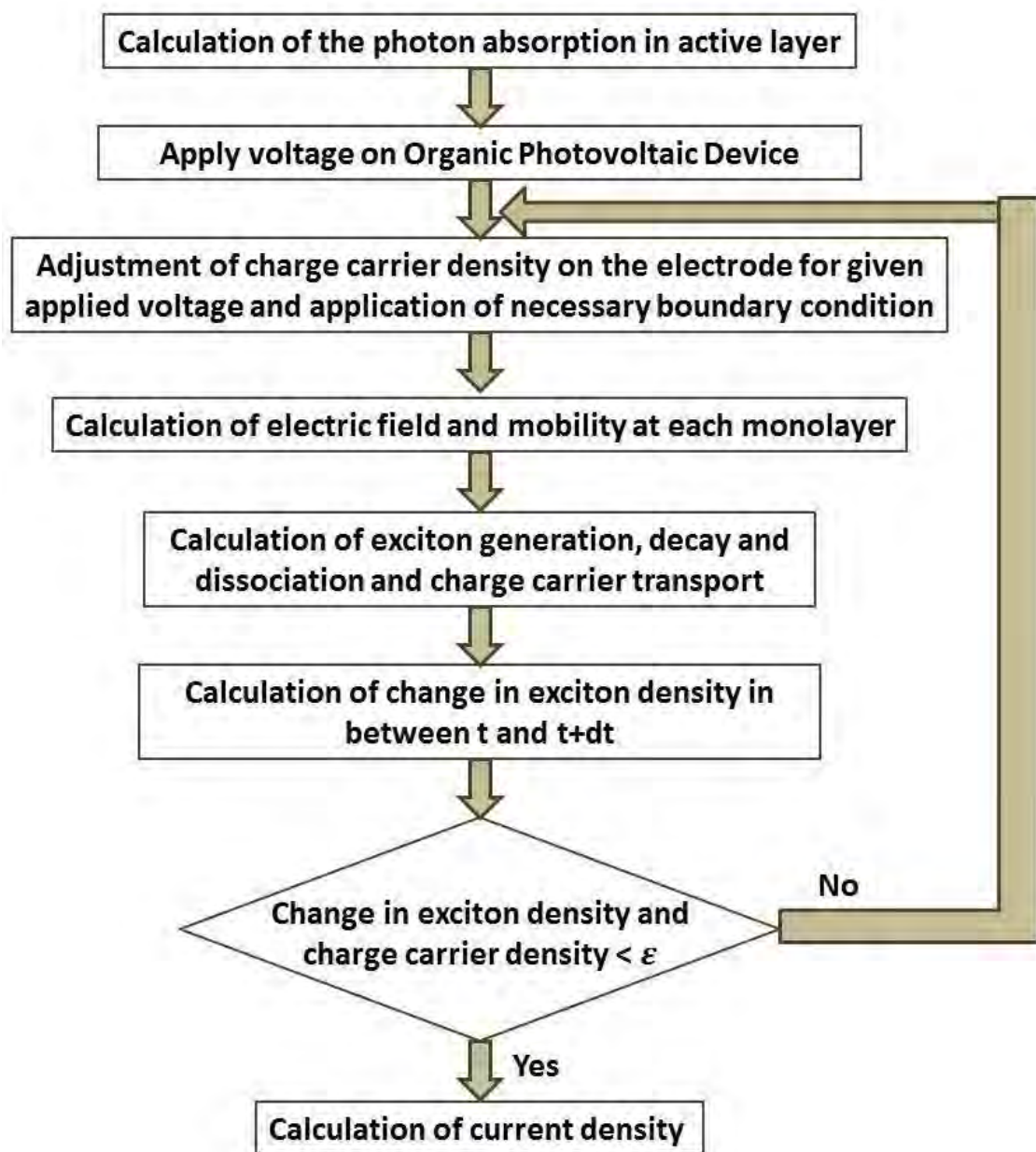


FIGURE 3.9 Flow chart of the proposed model

At first the photon generation rate of a P3HT:PCBM solar cell is calculated. For the simulation of this BHJ solar cell refractive indices data are taken from [75] and AM 1.5G irradiance data is taken from [76].

From Figure 3.10, it is seen that there is an oscillating nature in the generation rate. The oscillating nature with the thickness is found out due to the effect of interference and reflectance. So the total generation rate is calculated. Now with this generation rate exciton generation rate can be calculated.

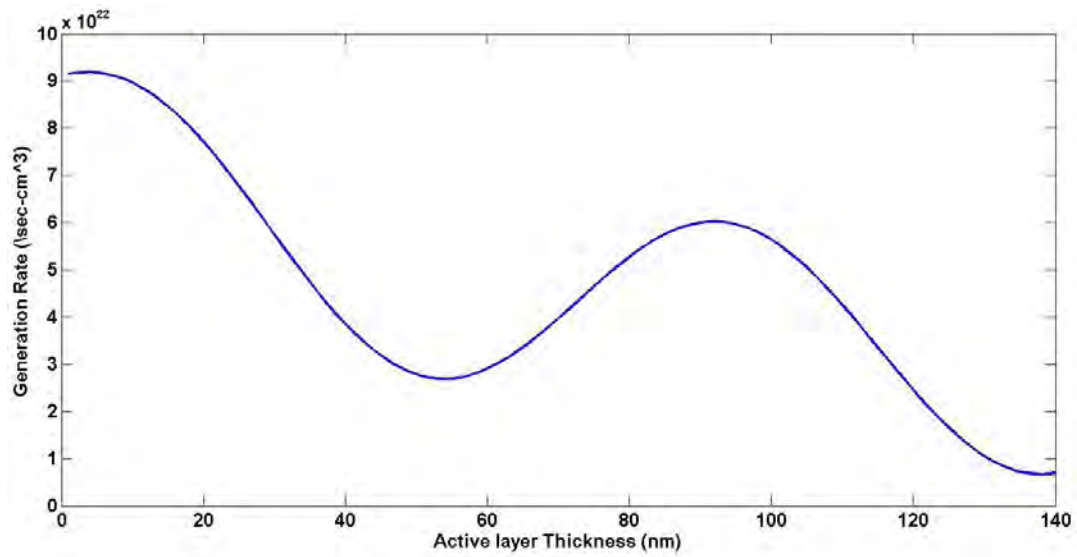


FIGURE 3.10 Generation rate of excitons in P3HT:PCBM bulk heterojunction solar cell

Then absorption rate of different layer of solar cell is simulated. The resultant figure is shown below:

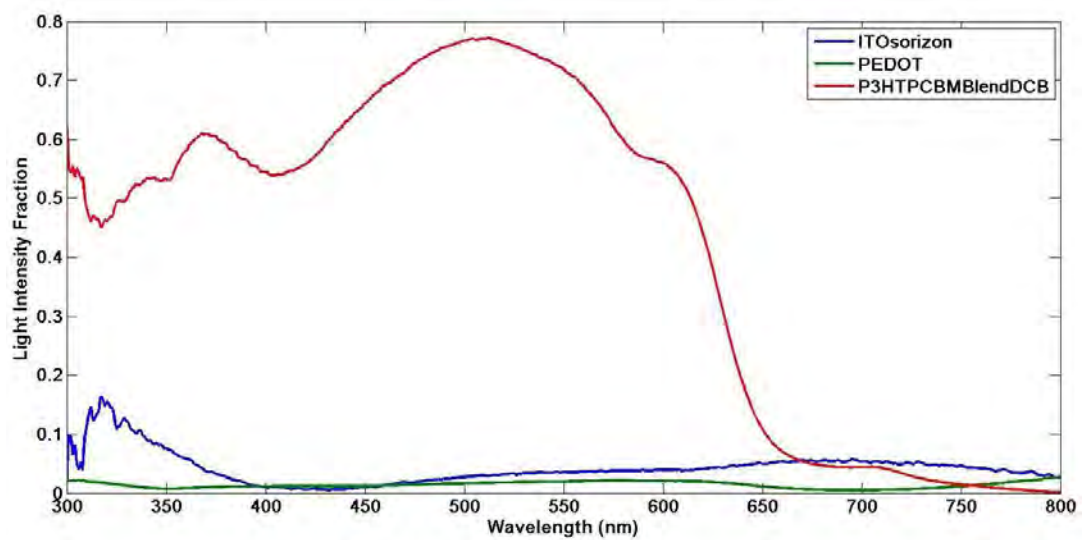


FIGURE 3.11 Absorption rate of different layer of P3HT:PCBM solar cell

From the Figure 3.11 it is seen that most of the absorption is taken place in P3HT:PCBM layer as expected.

3.4 Results of Electrical Modeling

Electrical modeling is performed to find out the J-V characteristics of the device. A couple of organic bulk heterunction solar cell is modeled using the proposed method. Again, sensitivity of different parameters to the current-voltage characteristics will be shown. In this section these results will be presented.

3.4.1 Variation of Active Layer Thickness

In this thesis active layer thickness is varied and its effect on the current-voltage characteristics is measured. This model is based on electric field dependent carrier mobility. So when active layer thickness is varied, as length is varied between the applied voltage, so electric field will change in the active layer. This model deals with the changed mobility. So when electric field is changed, mobility is changed according to Poole-Freknel equation. And as this model is concentrated on electric field dependent mobility, so change in electric field and its impact on the device performance with changed mobility is the important aspect for the validity of this model. As a result, device performance with active layer thickness is studied thoroughly and the result is compared with the existing model and experimental results.

For P3HT:PCBM solar cell in Figure 3.8 active layer thickness is varied by simulation. P3HT:PCBM solar cell is the most used organic solar cell in recent times. To find out the effect of active layer thickness in P3HT:PCBM solar cell, active layer thickness is varied from 40 nm to 140 nm. It will be better if more thickness can be simulated. For all this simulation dielectric constant is kept at 3.4, initial separation distance is kept at 1.07 nm, zero field electron mobility is kept at $1 \times 10^{-3} \text{cm}^2/\text{V.s}$, zero field electron mobility is kept at $1 \times 10^{-4} \text{cm}^2/\text{V.s}$ and effective density of states is kept at $1 \times 10^{18} \text{cm}^{-3}$. Decay rate is maintained at 1.5×10^6 per second. Convergence parameter is 0.2. Applied voltage is varied and corresponding current density is calculated with the proposed model. The obtained current-voltage characteristics is shown in the Figure 3.12.

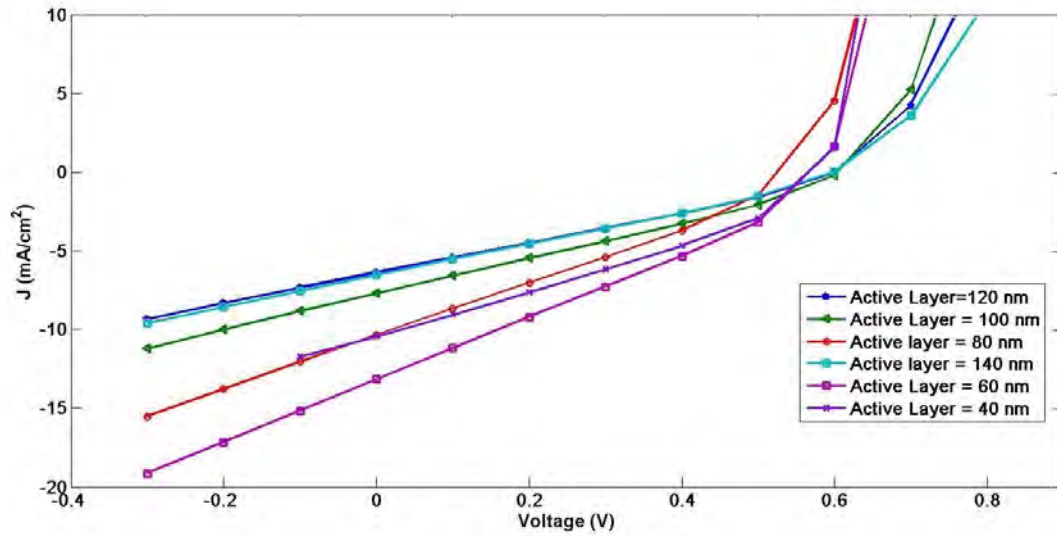


FIGURE 3.12 J-V characteristics with a variation of active layer thickness

From the obtained current-voltage characteristics it is seen that Fill Factor is not so great for the device. Open Circuit Voltage (V_{oc}), Short Circuit Current J_{sc} and Fill Factor can be obtained from the resultant current voltage characteristics.

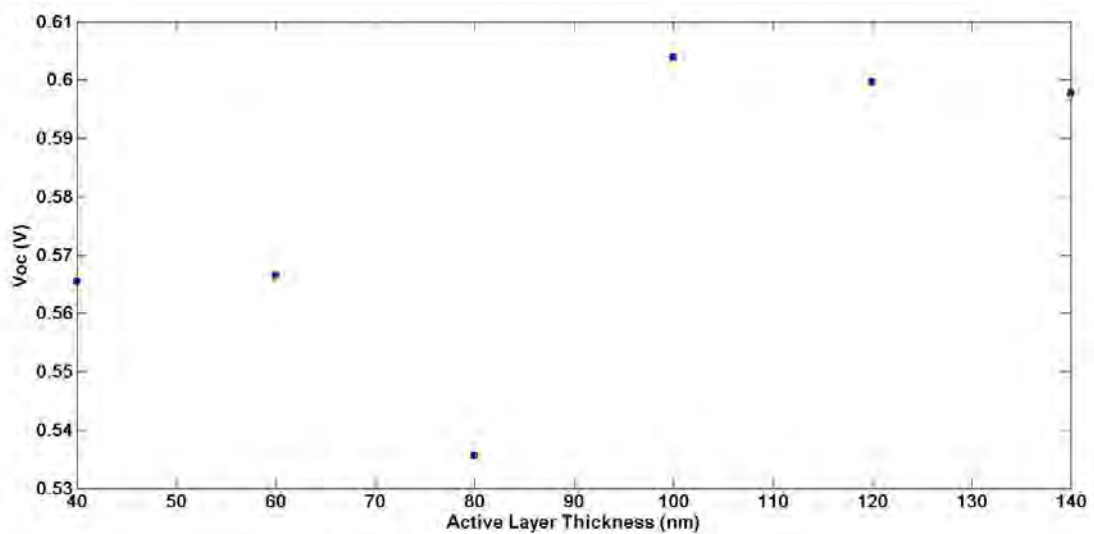


FIGURE 3.13 Voc with a variation of active layer thickness

From the obtained open circuit voltage in Figure 3.13, it is seen that open circuit voltage remains constant at around 0.6 V. which is consistent with experimental results in [77] and other models [62, 78]. The consistency in open circuit voltage can easily be understood as it has been known that V_{oc} depends on the energy

levels of donor and acceptor. So variation in active layer thickness doesn't change the open circuit voltage.

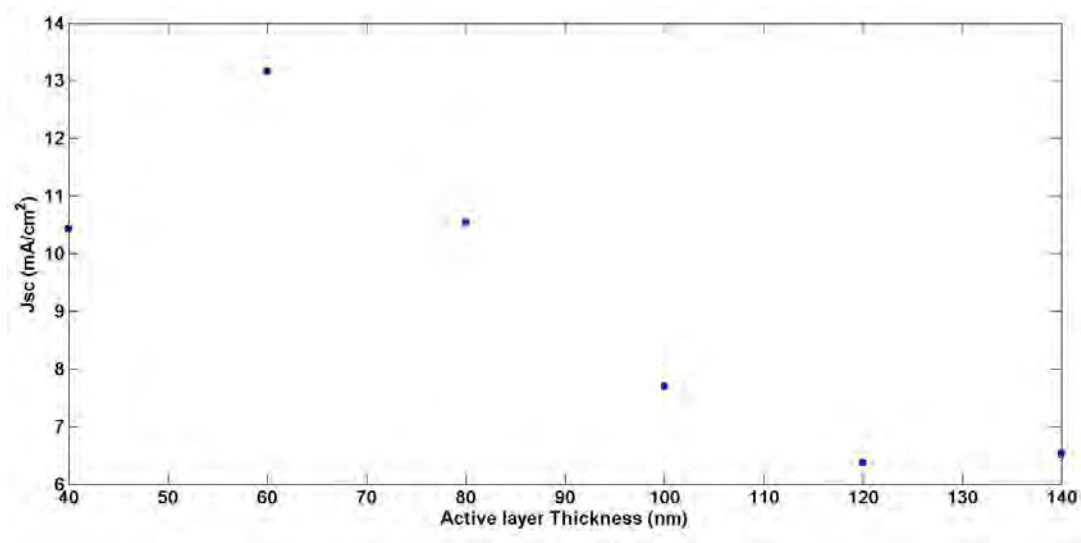


FIGURE 3.14 Short Circuit Current with a variation of active layer thickness

From Figure 3.14, it can be observed that contrary to V_{oc} , the short-circuit current J_{sc} of the device changes dramatically with the thickness of the active layer. The plot of short circuit current versus thickness shows two maxima at 60 nm when thickness is varied from 40 nm to 140 nm. At the 120 nm and 140 nm it almost constant which indicates that the value will rise further and get another maxima. This is consistent with the experimental results obtained in [77] and other models in [62, 78]. Since the number of photons absorbed in the active layer shows an oscillatory nature as the thickness of active layer increases (Figure 3.10), the short circuit current of the model devices also shows oscillatory behavior, because the photocurrent of solar cells depends on the number of photons absorbed in the active layer. However, the photocurrent at higher active layer thickness may not be consistent with the number of absorbed photons. Lower current density in active layer can then be attributed to the following two reasons: as the thickness of active layer increases, the electric field inside the active layer decreases at the constant bias voltage. Since the exciton dissociation rate depends on the electric field, the dissociation rate of excitons becomes smaller at lower electric field. Another possible reason for the decrease of short circuit current in thicker active layer is an increase in the recombination rate. Since a thicker device has longer pathway for

charge collection, it is easily expected that the probability for separated charges to recombine increases. Furthermore, due to lower electric field within thicker device under the short-circuit condition, the drift of charge carriers becomes slower and therefore the chance of recombination would be increased. The fraction of recombination events can be evaluated from the ratio of the recombination rate to the dissociation rate under the steady state. Thus, smaller short-circuit current density in thicker device is mainly attributed to an increase of the recombination rate.

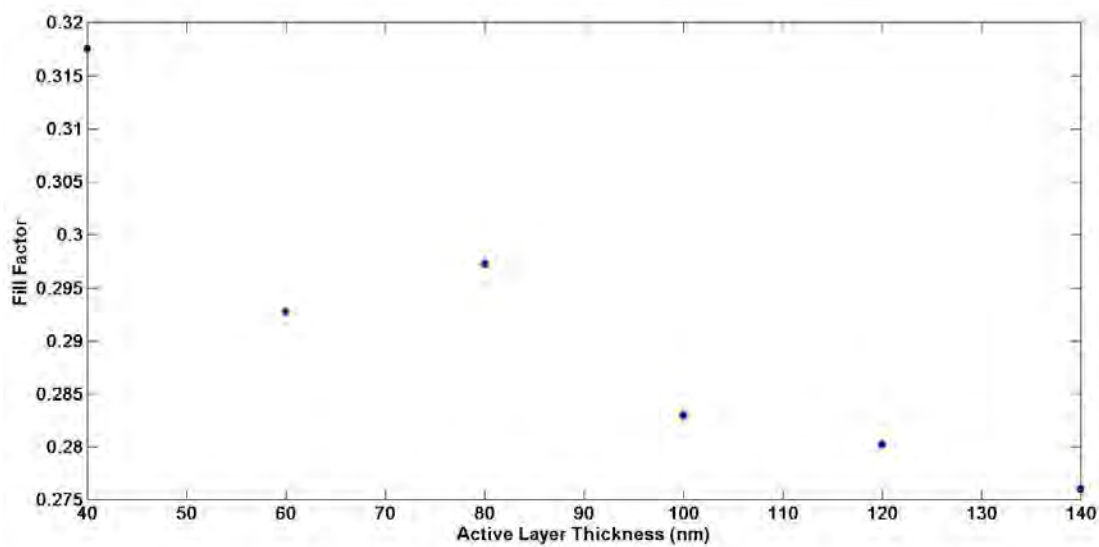


FIGURE 3.15 Fill Factor with a variation of active layer thickness

Fill factor of the device in Figure 3.15 is shown. Fill factor tends to decrease as the active layer thickness decreases which is in consistent with [79]. It can be attributed the fact that the recombination at maximum power point is more prominent in thicker device.

So from the Figure 3.16, it is seen that efficiency of the solar cell is maximum at 60 nm which is in match with experimental result [77]. It can be attributed to the fact that at 60 nm short circuit current is maximum and open circuit voltage is almost constant for all thickness. Though Fill factor decreases slightly but short circuit current dominates more and efficiency is maximum at layer thickness = 60 nm.

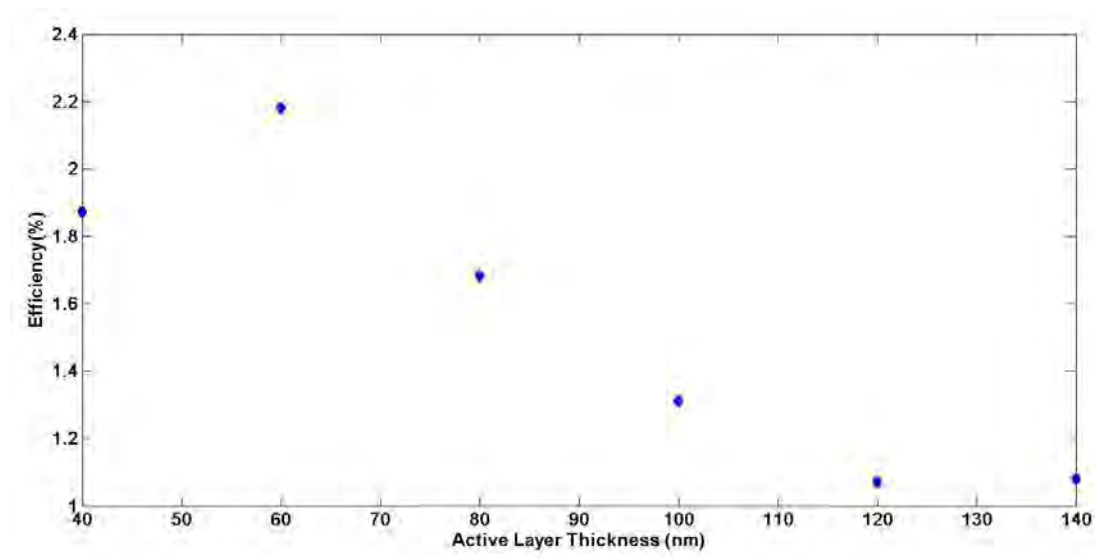


FIGURE 3.16 Efficiency with a variation of active layer thickness

3.4.2 Effect of Addition of Higher Mobility Solvent, CNT

Electron and Hole mobility can play an important role on device performance. This model is based on consideration of electric field dependent mobility. Now as an organic semiconductor mobility of the material will not be the same with the change in electrical field. In previous models, mobility is considered to be constant with the variation in electric field in order to assume the performance. But for determining the actual happening in the device electric field dependent mobility should be considered. Moreover, addition of different solvent can alter the mobility curve of the active layer. So, in this section, performance of higher mobility solvent is analysed.

Carbon Nano Tube (CNT) is a promising material in organic solar cell. It is used as a solvent in the active layer by researcher experimentally [80–82]. So in this part, performance analysis of nominal solar cell and CNT doped solar cell is analysed. It is reported that by the addition of CNT in the active layer absorption is almost unchanged [80]. Now by adding CNT as a solvent the hole mobility of the active layer increases to $1.5 \times 10^{-3} \text{cm}^2/\text{V.s}$. So the performance of the solar cell with the addition of CNT is shown the figure below.

As absorption is almost same with the addition of CNT, so optical modeling remains same as previous. For electrical modeling as hole mobility is changed, so hole mobility is used from [80] for CNT doped P3HT:PCBM solar cell. Using this hole mobility and 140 nm active layer thickness current-voltage characteristics is calculated. All other parameters remain same as previous.

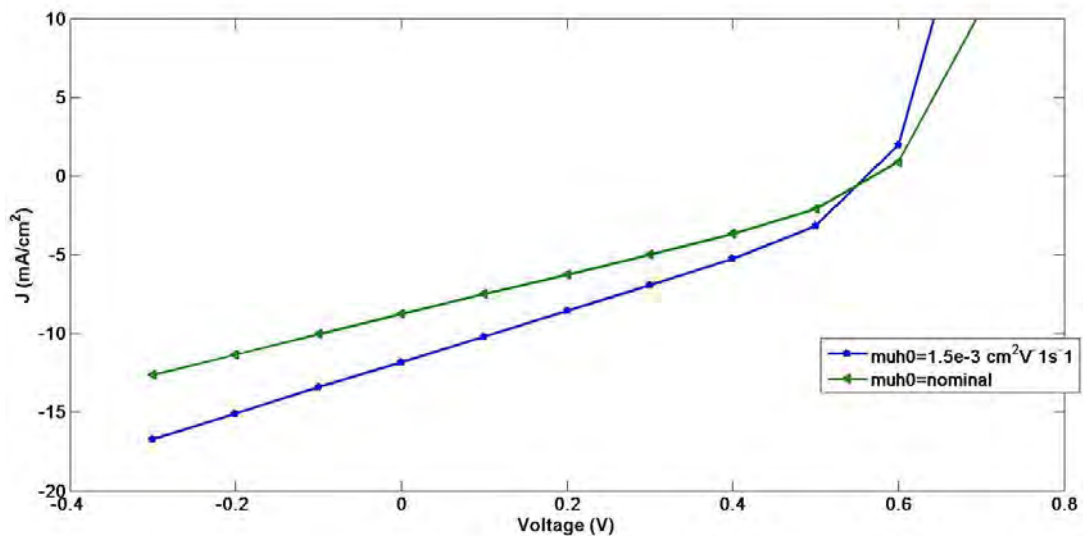


FIGURE 3.17 Current-Voltage characteristics with a variation of hole mobility

It is evident from Figure 3.17, that performance is definitely improved by the addition of CNT. In order to have a closer look at the device performance, open circuit voltage, short circuit current and fill factor is shown in Figure 3.18, 3.19 and 3.20 respectively.

From the results it is expected that the efficiency of the solar cell will be improved by the addition of CNT as solvent. The efficiency of the solar cell before adding CNT and after addition of CNT is shown in Table 3.1. So, the result is as expected.

TABLE 3.1 Efficiency of solar cell with and without CNT

	Without CNT	With CNT
Efficiency (%)	1.5	2.1

So it is seen that efficiency is increased about 40% with the addition of Carbon Nano Tube as solvent in the active layer.

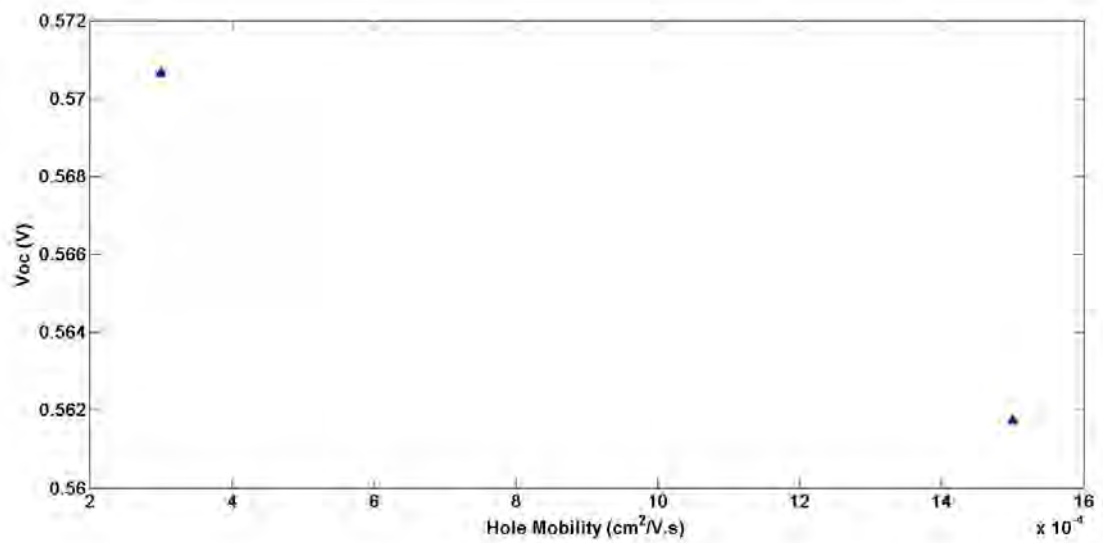


FIGURE 3.18 Open circuit voltage with a variation of hole mobility

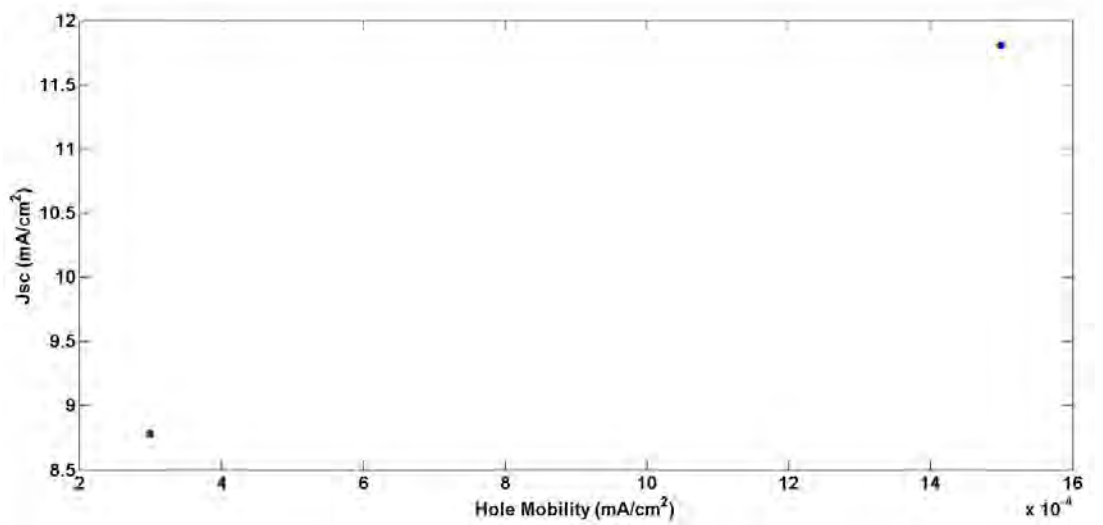


FIGURE 3.19 Short circuit current with a variation of hole mobility

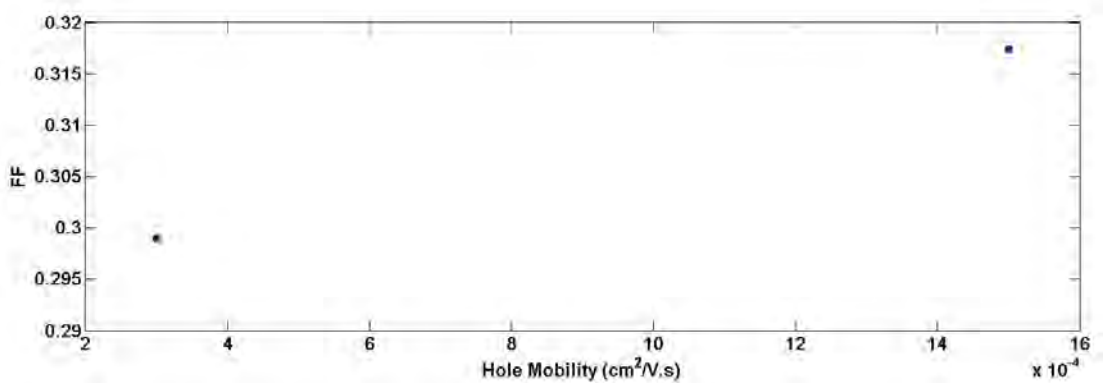


FIGURE 3.20 Fill factor with a variation of hole mobility

3.4.3 Effect of Donor Concentration on the Device Performance

Researchers always try to find a model to quantitatively describes the experimental data or propose new device design. In this section device performance with a variation in donor concentration is predicted for a TAPC: C_{60} bulk heterojunction solar cell. My model is used to model the effects of donor concentration on the device performance.

Now TAPC is a non-absorbing material in the visible spectrum. Thus the photon absorption can be attributed to C_{60} molecule. The absorption coefficient of the mixed layer can be defined as,

$$\alpha_{\lambda}(c_{TAPC}) = \alpha_{\lambda}(C_{60})(1 - (c_{TAPC})) \quad (3.31)$$

where $\alpha_{\lambda}(c_{TAPC})$ and $\alpha_{\lambda}(C_{60})$ are absorption coefficient of the mixed material and C_{60} respectively at wavelength λ and TAPC concentration c_{TAPC} . Since the photon absorption is calculated according to the transfer matrix theory where the complex refractive index (n,k) of the mixed material is required. Intuitively, I assume that,

$$k_{\lambda}(c_{TAPC}) = k_{\lambda}(C_{60})(1 - (c_{TAPC})) \quad (3.32)$$

where $k_{\lambda}(c_{TAPC})$ and $k_{\lambda}(C_{60})$ are imaginary part of the optical refractive index of the mixed material and C_{60} [83] respectively. Real part of the refractive index of the mixture is assumed to be same as C_{60} .

To find out the effect of donor concentration in TAPC:C60 solar cell, donor concentration is varied from 25% to 50%. It will be better if more thickness can be simulated. For all this simulation dielectric constant of the mixed structure is calculated using the following relation [84],

$$\epsilon_r(c_{TAPC}) = (c_{TAPC} * \epsilon_r(TAPC)^{1/3} + (1 - c_{TAPC}) * \epsilon_r(C60)^{1/3})^3 \quad (3.33)$$

where $\epsilon_r(C60)$ [85] and $\epsilon_r(TAPC)$ [86] are the dielectric constants of C60 and TAPC respectively. Dielectric constant of TAPC is 3.5 and C60 is 4.5. Increase in the TAPC concentration will lower the dielectric constant of the material and increases the Coulomb force between the charge pairs in CT states. Consequently, the dissociation of CT states becomes more difficult [87].

Initial separation distance is kept at 1.1 nm, zero field electron mobility is kept at $1 \times 10^{-3} cm^2/V.s$, zero field electron mobility is kept at $1 \times 10^{-4} cm^2/V.s$ and effective density of states is kept at $1 \times 10^{18} cm^{-3}$. Decay rate is maintained at 5×10^6 per second. Convergence parameter is 0.2. Applied voltage is varied and corresponding current density is calculated with the proposed model. The obtained current-voltage characteristics is shown in the Figure 3.21.

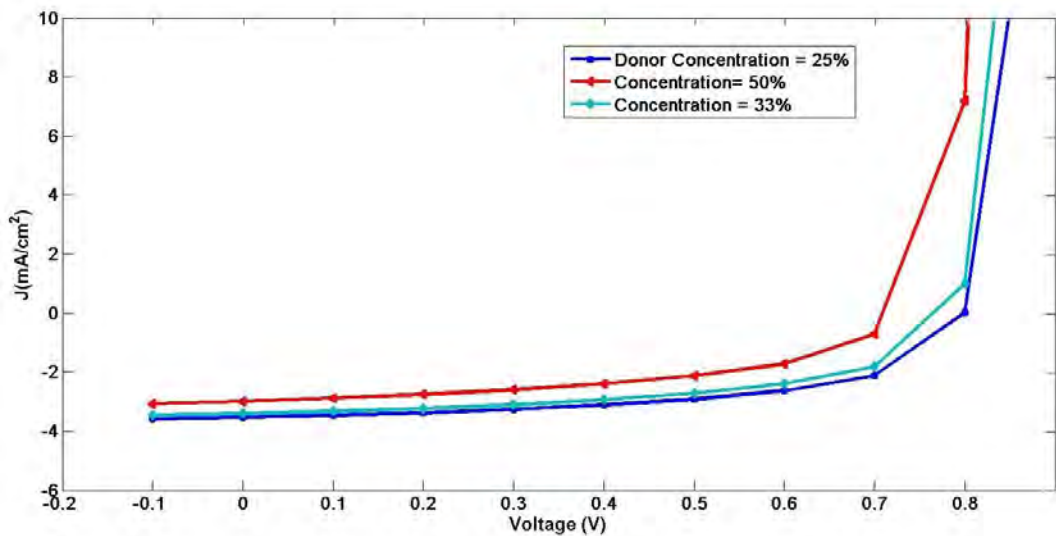


FIGURE 3.21 Current voltage characteristics with a variation of donor concentration

In order to watch the effect of donor concentration closely on the device performance, open circuit voltage and short circuit current of the device are plotted separately for variation in donor concentration.

From the figure it is seen that at the higher concentration of TAPC both V_{oc} and J_{sc} decrease. It can be attributed to the reduction in dielectric constant and electron

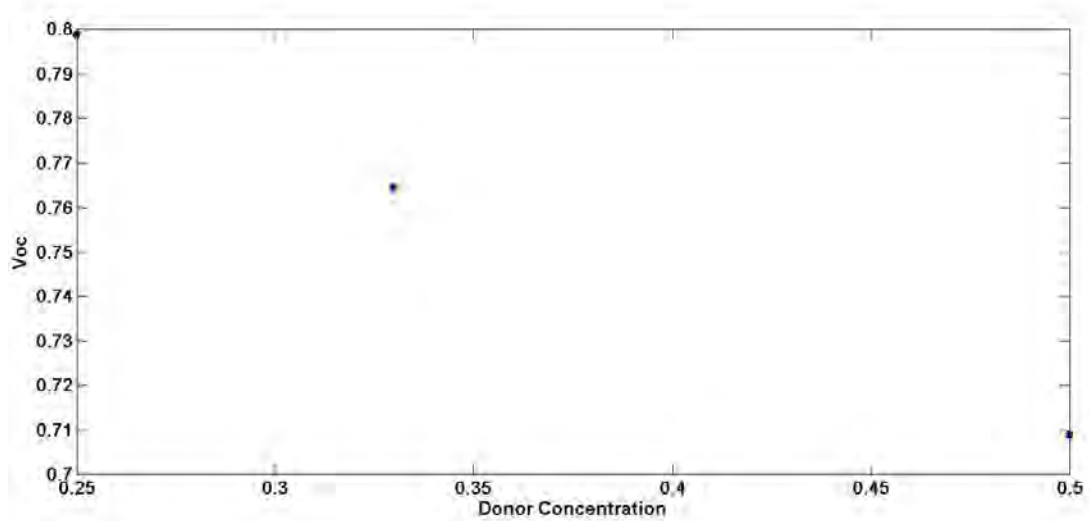


FIGURE 3.22 Open circuit voltage with a variation of donor concentration

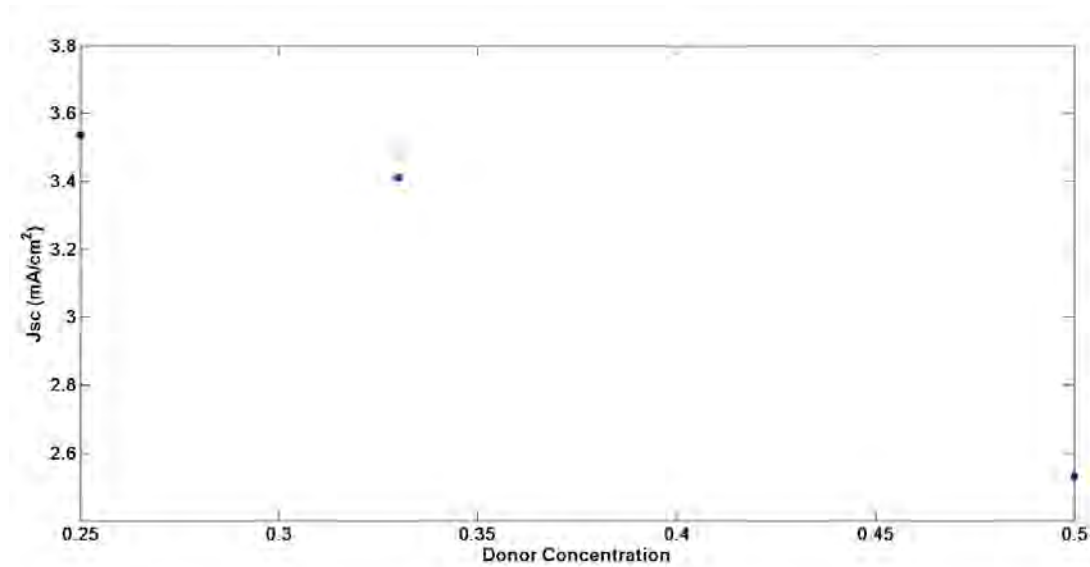


FIGURE 3.23 Short Circuit Currents with a variation of donor concentration

mobility of the TAPC:C60 layer becomes significant and adversely affecting the J_{sc} and FF. The efficiency of the TAPC solar cell with the change in concentration is shown in the Table 3.2.

TABLE 3.2 Efficiency of solar cell with donor concentration

Donor Concentration (%)	Efficiency
25	1.58
33	1.44
50	1.06

3.5 Sensitivity to the Parameters

As this model is a numerical model it uses a couple of fitting parameters to match the experimental results. In this section sensitivity to the various fitting parameter is analysed.

3.5.1 Sensitivity of effective density of states

In order to find out the effect of effective density of states, this parameter is varied. Higher density of states of carriers near contacts, will create band bending and effectively reduces the field and hence mobility is also changed according to it. The impact of this phenomena on current-voltage characteristics is shown in Figure 3.24

In order to investigate more about the open circuit voltage, short circuit current and fill factor these performances are plotted individually. Figure 3.25, Figure 3.26 and Figure 3.27 shows the effect of density of states on these parameters respectively.

From Figure 3.25, it is seen that open circuit voltage decreases with the increase in effective density of states. It can be attributed to the fact that at low density of states there is uniform built in electric field throughout the device. But at higher density of states there is band bending near the contact as there is high majority charge carrier density near the contacts in this case. Due to band bending, electric

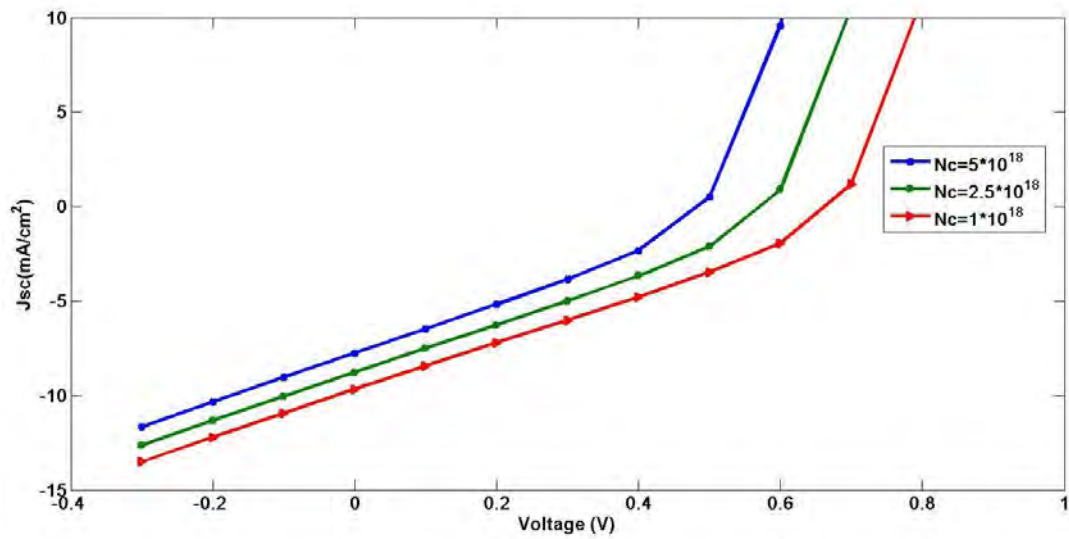


FIGURE 3.24 Current Voltage Characteristics with a variation of effective density of states

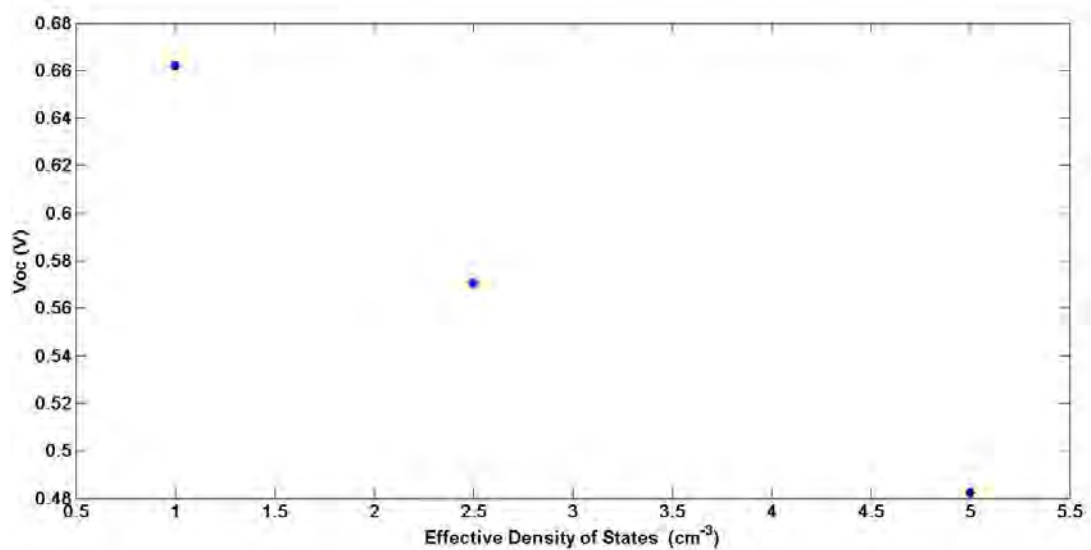


FIGURE 3.25 Open circuit voltage with a variation of effective density of states

field is reduced and consequently open circuit voltage is reduced at higher effective density of states.

It is seen from Figure 3.26 that, short circuit current also decreases with the increase in effective density of states. The same reason as for V_{oc} can also be attributed here. Due to low electric field at higher effective density of states short circuit current reduces.

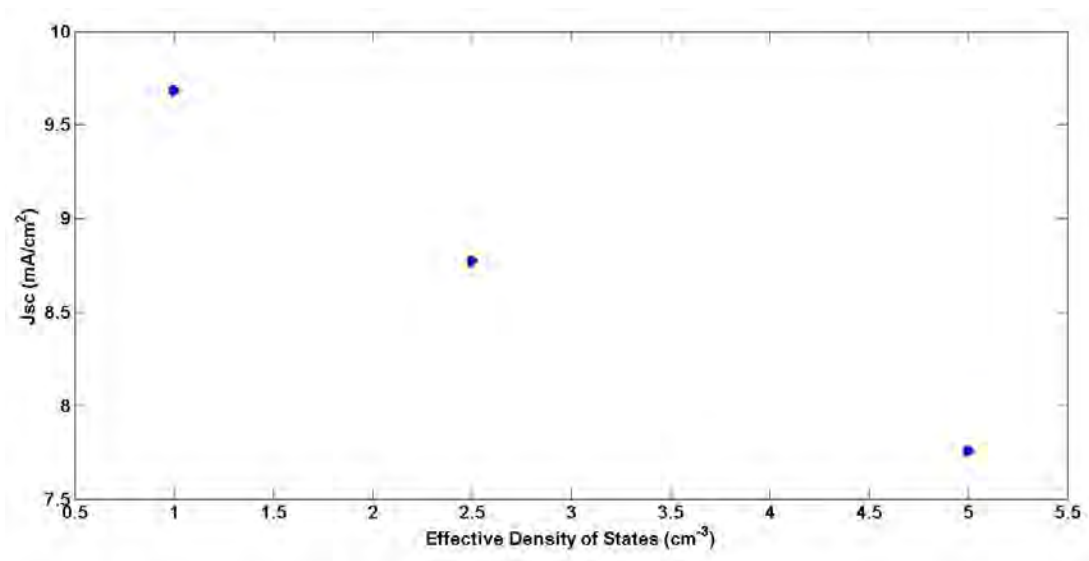


FIGURE 3.26 Short circuit current with a variation of effective density of states

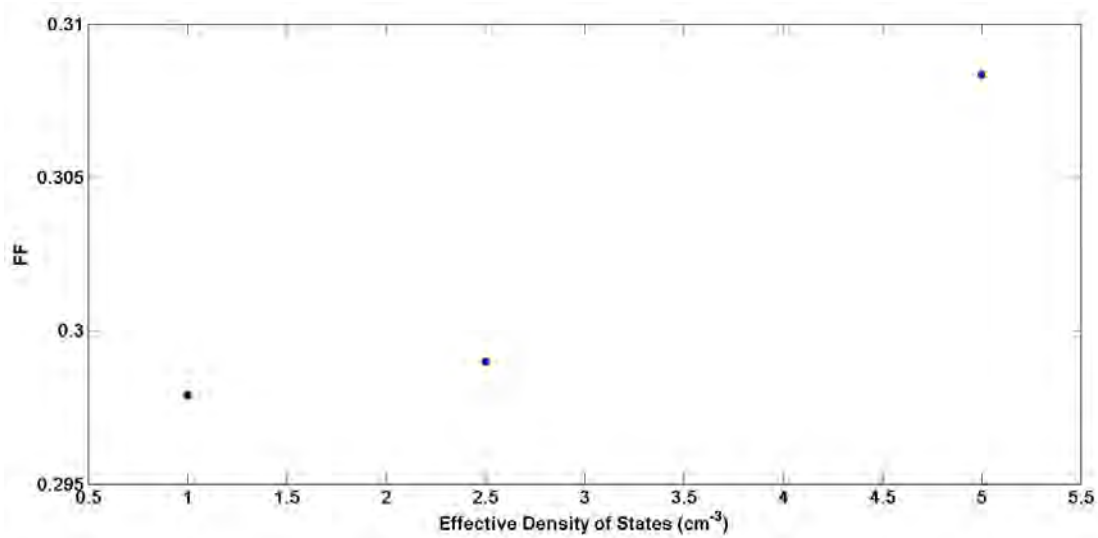


FIGURE 3.27 Fill factor with a variation of effective density of states

From Figure 3.27, it is seen that fill factor increases with the increase in effective density of states.

3.5.2 Sensitivity of Initial Separation Distance

Initial separation distance is the distance between electron and hole of the bound exciton. In some model Gaussian spatial distribution of critical separation distance is used. But in this model critical separation distance of every exciton is assumed

to be same and a single constant value. Now, the impact of this fitting parameter in the device performance is simulated. Resultant curve is shown in Figure 3.28.

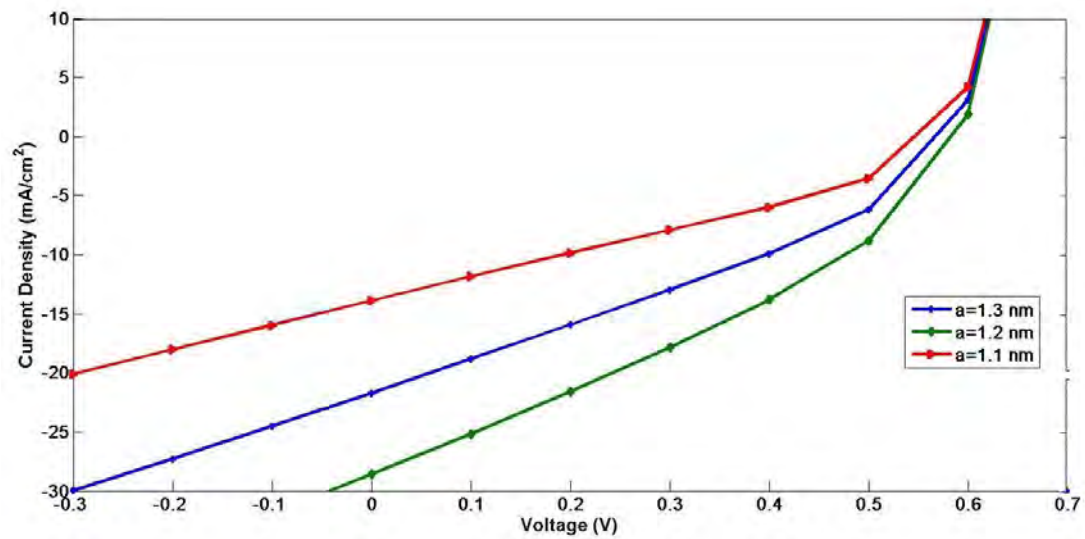


FIGURE 3.28 Current Voltage characteristics with a variation of initial separation distance

It is seen that for 1.2 nm of initial separation distance short circuit current is maximum. As dissociation rate of CT state depends on the initial separation distance, so a larger separation distance tends more exciton to dissociate and hence more electron-hole pair. So the result follows.

Chapter 4

Conclusion and Suggestions

4.1 Conclusion

Many solar cell technologies exist for the direct conversion of light into electricity, each with its own advantages and disadvantages. One of the most important quantity for determining the competitiveness of different solar cell technology is the expected cost per kWatt produced. There are many strategies being pursued to achieve cost efficiency such as improving efficiency of standard silicon cells, reducing the amount of expensive raw materials with thin films, developing lower cost manufacturing methods, and designing high efficiency devices with small areas. Organic solar cells are a newer technology in this field and have the potential for low manufacturing and material costs. However, organic semiconductors are still a relatively new field with unique great properties. But still many of them are still unknown and researchers are exploring the new fields of organic solar cells. Various experimental and theoretical work have been done by the researcher. To predict the device performance not only the experimental work but also modeling is necessary. With device modeling one can measure many properties which are too expensive to measure or need a great amount of time and propose new device design.

As mobility of the organic material is not constant for all electric field, so a model considering electric field dependent mobility is necessary to explore. In this thesis bulk heterojunction organic solar cell is modeled considering the aforementioned fact. For the modeling purpose complex refractive index of the organic materials are taken as input and using this total photon absorption at depth of active layer is obtained using transfer matrix formalism considering AM 1.5G irradiance. An oscillating nature of photon absorption is found for the organic solar cell due to the interference and reflectance effect of the layers. After the calculation of photon absorption rate, exciton generation rate is assumed to same as photon absorption rate as Donor acceptor interface is uniformly distributed everywhere in bulk heterojunction device. Exciton transfer to charge transfer state where they either dissociate or decay. Decay rate is assumed to be constant and dissociation rate depends on the electric field and initial separation distance of electron and hole in exciton. After the dissociation of excitons electrons and holes are generated and their transport is modeled by continuity equation. Current in the device is considered to be drift diffusion current and field dependent mobility is considered to model the BHJ organic solar cell.

At first, bilayer organic solar cell is simulated using simulator and it is found that the efficiency of this solar cell is too low as expected. From variation in acceptor thickness, donor thickness and mobility, the maximum efficiency of around 0.9% is achieved. After that, P3HT:PCBM bulk heterojunction solar cell is simulated with a variation of active layer thickness. As this model is based on field dependent carrier mobility, so change in layer thickness subsequently changes electric field and hence model can be verified. It is observed that at 60 nm efficiency is maximum when layer thickness is varied from 40 nm to 140 nm and it is expected that short circuit current will follow an oscillating nature like photon absorption profile. Open circuit voltage remains almost constant at 0.6 V for all thicknesses. Thereafter, the impact of a high hole mobility solvent in the active layer is examined. When a high mobility solvent CNT is added in P3HT:PCBM active layer, efficiency is increased by 40%. For TAPC:C60 bulk heterojunction solar cell, with the increase in C60 concentration open circuit voltage and short circuit current increases which

can be attributed to the less absorbing capability of TAPC. The model is sensitive to the effective density of states and initial separation distance. With the increase in effective density of states, the current voltage curve shifts to the left meaning both open circuit voltage and short circuit current decreases. It can be attributed to the band bending near contact region at high effective density of states. The device performance also varies with the initial separation distance between electron and hole in the exciton.

4.2 Suggestions

Mobility of the organic solar cell is changes with the annealing and morphological changes. As this model has the capability of taking variable mobility, so not only electric field but also annealing and morphology dependent mobility of the organic compound can be considered to model bulk heterojunction organic solar cell. Moreover, with the experimental knowledge of refractive index of the materials, dielectric constant and mobility of the compound any organic solar cell can be modeled using the proposed model. First principle study of the morphological dependence of the mobility can be obtained in future and incorporating this model with the first principle study, a better model can be achieved.

Appendix A

Simulation Codes

A.1 Sample Code for Optical Modeling

```
althick=40;%in nm
lamda = 300:10:900; %in nm
stepsize = 1;
layers = {'SiO2' 'ITO sorizon' 'MoOx' 'C60' 'Bphen' 'Al'};
thickness = [0 100 3 althick 8 100];
activeLayer = 4;

AM15_data=xlsread('AM15.xls');
AM15=interp1(AM15_data(:,1), AM15_data(:,2), lamda, 'linear', 'extrap');

ntotal = zeros(size(layers,2),size(lamda,2));
for index = 1:size(layers,2)
    [IndRefr,IndRefr_names]=xlsread('Index_of_Refraction_library.xls');
    file_wavelengths=IndRefr(:,strmatch('Wavelength',IndRefr_names));
    nr=IndRefr(:,strmatch(strcat(layers{index},'_n'),IndRefr_names));
    if index==4
```

```

        k=IndRefr(:,strmatch(strcat(layers{index},'_k'),IndRefr_names))*(1-ch);
    else
        k=IndRefr(:,strmatch(strcat(layers{index},'_k'),IndRefr_names));
    end
    ntotal(index,:) = nr+li*k;
end
t(1) = 0;
t_cumsum = cumsum(thickness);
nfull=zeros(size(ntotal,1),size(lamda));
track_n=1;
for m=1:length(lamda)
    nfull(1,m)=ntotal(1,m);
end
for m=2:length(thickness)
    dj=thickness(m);
    nfull(track_n+1:track_n+dj,:)=repmat(ntotal(m,:),dj,1);
    track_n=track_n+dj;
    size(nfull)
end
nfull(size(nfull,1)+1,:)=1;

G=zeros(size(nfull,1)-1,length(lamda));
for m = 1:length(lamda)
    for pp=1:size(nfull,1)-1
        I11(pp)=(nfull(pp,m)+nfull(pp+1,m))/(2*nfull(pp,m));
        I22(pp)=I11(pp);
        I12(pp)=(nfull(pp,m)-nfull(pp+1,m))/(2*nfull(pp,m));
        I21(pp)=I12(pp);
    end
    for pp = 2:size(nfull,1)-1
        xi=2*pi*nfull(pp,m)/lamda(m);

```

```

    L11(pp)=exp(-1i*xi);
    L22(pp)=exp(1i*xi);
    L12(pp)=0;
    L21(pp)=0;
end
S11(2)=I11(1);S12(2)=I12(1);S21(2)=I21(1);S22(2)=I22(1);
for pp=3:size(nfull,1)
    t1=S11(pp-1)*L11(pp-1)+S12(pp-1)*L21(pp-1);
    t2=S11(pp-1)*L12(pp-1)+S12(pp-1)*L22(pp-1);
    t3=S21(pp-1)*L11(pp-1)+S22(pp-1)*L21(pp-1);
    t4=S21(pp-1)*L12(pp-1)+S22(pp-1)*L22(pp-1);

    S11(pp,m)=t1*I11(pp-1)+t2*I21(pp-1);
    S12(pp,m)=t1*I12(pp-1)+t2*I22(pp-1);
    S21(pp,m)=t3*I11(pp-1)+t4*I21(pp-1);
    S22(pp,m)=t3*I12(pp-1)+t4*I22(pp-1);
end
Ep(1,m)=1;En(size(nfull,1),m)=0;
En(1,m)=Ep(1,m)*S21(size(nfull,1),m)/S11(size(nfull,1),m);
Ep(size(nfull,1),m)=Ep(1,m)/S11(size(nfull,1),m);
R1(m)=(1-nfull(1,m))*(1-nfull(1,m))/(1+nfull(1,m))/(1+nfull(1,m));
R2(m)=abs(S21(size(nfull,1))/S11(size(nfull,1),m))^2;
qx=zeros(length(nfull)-1,length(lambda));
absorp=zeros(length(nfull)-1,length(lambda));
for pp=2:size(nfull,1)-1
    Ep(pp,m)=(S22(pp,m)*Ep(1,m)-S12(pp,m)*En(1,m))/(S11(pp,m)*S22(pp,m)
        -S12(pp,m)*S21(pp,m));
    En(pp,m)=(-S21(pp,m)*Ep(1,m)+S11(pp,m)*En(1,m))/(S11(pp,m)*S22(pp,m)
        -S12(pp,m)*S21(pp,m));
    mod_Esq(pp,m)=abs(Ep(pp,m)+En(pp,m))^2;
    absorp(pp,m)=4*pi*(1-R1(m))/(lamda(m)*nfull(1,m)*(1-R1(m)*R2(m)));

```



```
        qx(pp,m)=absorp(pp,m)*imag(nfull(pp,m))*real(nfull(pp,m))*mod_Esq(pp,m)
        G(pp,m)=qx(pp,m)*AM15(m);
    end
end

diel_r=(ch*diel_r1^(1/3)+(1-ch)*diel_r2^(1/3))^3;

G1=sum(G,2);
G2=G1(105:104+althick);
figure(1);plot(G2*1e3/q);
```

A.2 Sample Code for Electrical Modeling

```

Ep0=Ep00*ones(althick+2,1);En0=En00*ones(althick+2,1);
mun0=mun00*ones(althick+2,1);mup0=mup00*ones(althick+2,1);

FF=0;pmax=0;Vpmax=0;Jpmax=0;Jsc=0;Joc=100;
Voc=0;Vocbot=0;Voctop=0;Jocbot=1000;Joctop=1000;

p=zeros(althick+2,1);n=zeros(althick+2,1);
F=zeros(althick+2,1);Fint=zeros(althick+2,1);
pnew=zeros(althick+2,1);nnew=zeros(althick+2,1);
Xnew=zeros(althick+2,1);X=zeros(althick+2,1);
R=zeros(althick+2,1);P=zeros(althick+2,1);
U=zeros(althick+2,1);jp=zeros(althick+2,1);jn=zeros(althick+2,1);
jt=zeros(althick+2,1);jpdiff=zeros(althick+2,1);jpdrift=zeros(althick+2,1);
jndrift=zeros(althick+2,1);jndiff=zeros(althick+2,1);
mun=zeros(althick+2,1);mup=zeros(althick+2,1);
Dp=zeros(althick+2,1);Dn=zeros(althick+2,1);

nisq=Nc*Nv*exp(-Eg/kT);
p(3:althick)=4e17;
n(3:althick)=4e17;

V=Vbegin:dV:0.7;

for yy=1:length(V)

    VV=V(yy);
    p(2)=Nv; p(althick+1)=Nv*exp(-Eg/kT);
    n(2)=Nc*exp(-Eg/kT); n(althick+1)= Nc;

```

```

p(1)=n(2); n(1)=p(2);
p(althick+2)=n(althick+1);
n(althick+2)=p(althick+1);

flag=0;

% Electrical Field Calculation
for mm=1:althick+1
    Fint(mm)=0;
    for pp=1:althick+2
        if pp<=mm
            Fint(mm)=Fint(mm)+dl*q*(p(pp)-n(pp))/2/diel_0/diel_r;
        else
            Fint(mm)=Fint(mm)-dl*q*(p(pp)-n(pp))/2/diel_0/diel_r;
        end
    end
end
end
for mm=2:althick+1
    F(mm)=(Fint(mm-1)+Fint(mm))/2;
end
VF=sum(F.*dl);
VF=Vbi+VF;
n(1)=n(1)+(VF-VV)*diel_0*diel_r/(q*dl*althick*dl);
p(althick+2)=p(althick+2)+(VF-VV)*diel_0*diel_r/(q*dl*althick*dl);
if n(1)<p(1)
    p(1)=p(1)-n(1);n(1)=0;
else
    n(1)=n(1)-p(1);p(1)=0;
end
end
if n(althick+2)<p(althick+2)

```

```

        p(althick+2)=p(althick+2)-n(althick+2);n(althick+2)=0;
    else
        n(althick+2)=n(althick+2)-p(althick+2);p(althick+2)=0;
    end
    for mm=2:althick+1
        F(mm)=F(mm)-(VF-VV)/althick/dl;
        mun(mm)=mun0(mm)*exp(En0(mm)*sqrt(abs(F(mm))));
        Dn(mm)=mun(mm)*kT;
        mup(mm)=mup0(mm)*exp(Ep0(mm)*sqrt(abs(F(mm))));
        Dp(mm)=mup(mm)*kT;
    end
    F
    x=[abs(mun.*F); abs(mup.*F);abs(Dn/dl);abs(Dp/dl)];
    mufmax=max(max(x));
    dt=dl/mufmax/ts_factor;

    for iter=1:Nmax
        iter,flag,yy
    if flag==0

        flag=1;
        dpp=0;dnn=0;

        for gg=3:althick
            pnew(gg)=p(gg)+dt*((Dp(gg+1)*p(gg+1)+Dp(gg-1)*p(gg-1)-2*Dp(gg)
                *p(gg))/(dl*dl)-p(gg)*mup(gg)*abs(F(gg))/dl);
            if (F(gg+1)<0)
                pnew(gg)=pnew(gg)+dt*p(gg+1)*mup(gg+1)*abs(F(gg+1))/dl;
            end
            if (F(gg-1)>0)

```

```

        pnew(gg)=pnew(gg)+dt*p(gg-1)*mup(gg-1)*abs(F(gg-1))/dl;
    end

    nnew(gg)=n(gg)+dt*((Dn(gg+1)*n(gg+1)+Dn(gg-1)*n(gg-1)-2*Dn(gg)
        *n(gg))/(dl*dl)-n(gg)*mun(gg)*abs(F(gg))/dl);
    if (F(gg+1)>0)
        nnew(gg)=nnew(gg)+dt*n(gg+1)*mun(gg+1)*abs(F(gg+1))/dl;
    end
    if (F(gg-1)<0)
        nnew(gg)=nnew(gg)+dt*n(gg-1)*mun(gg-1)*abs(F(gg-1))/dl;
    end

end

gg=2;
pnew(gg)=p(gg)+dt*((Dp(gg+1)*p(gg+1)-Dp(gg)*p(gg))/(dl*dl));
if (F(gg+1)<0)
    pnew(gg)=pnew(gg)+dt*p(gg+1)*mup(gg+1)*abs(F(gg+1))/dl;
end
if (F(gg)>0)
    pnew(gg)=pnew(gg)-dt*p(gg)*mup(gg)*abs(F(gg))/dl;
end

nnew(gg)=n(gg)+dt*((Dn(gg+1)*n(gg+1)-Dn(gg)*n(gg))/(dl*dl));
if (F(gg+1)>0)
    nnew(gg)=nnew(gg)+dt*n(gg+1)*mun(gg+1)*abs(F(gg+1))/dl;
end
if (F(gg)<0)
    nnew(gg)=nnew(gg)-dt*n(gg)*mun(gg)*abs(F(gg))/dl;
end

```

```

gg=althick+1;
pnew(gg)=p(gg)+dt*((Dp(gg-1)*p(gg-1)-Dp(gg)*p(gg))/(dl*dl));
if (F(gg-1)>0)
    pnew(gg)=pnew(gg)+dt*p(gg-1)*mup(gg-1)*abs(F(gg-1))/dl;
end
if (F(gg)<0)
    pnew(gg)=pnew(gg)-dt*p(gg)*mup(gg)*abs(F(gg))/dl;
end

nnew(gg)=n(gg)+dt*((Dn(gg-1)*n(gg-1)-Dn(gg)*n(gg))/(dl*dl));
if (F(gg-1)<0)
    nnew(gg)=nnew(gg)+dt*n(gg-1)*mun(gg-1)*abs(F(gg-1))/dl;
end
if (F(gg)>0)
    nnew(gg)=nnew(gg)-dt*n(gg)*mun(gg)*abs(F(gg))/dl;
end

for gg=2:althick+1
    if (n(gg)*p(gg))>nisq
        R(gg)=q*(mun(gg)+mup(gg))*(n(gg)*p(gg)-nisq)/diel_0/diel_r;
    else
        R(gg)=0;
    end
    Xnew(gg)=X(gg)+dt*(G2(gg-1)/(dl*q*1000)-kf*X(gg)-kd(mun(gg)
        +mup(gg),a,diel_r,F(gg))*X(gg)+R(gg));
    pnew(gg)=pnew(gg)-R(gg)*dt+kd(mun(gg)+mup(gg),a,diel_r,F(gg))
        *X(gg)*dt;
    nnew(gg)=nnew(gg)-R(gg)*dt+kd(mun(gg)+mup(gg),a,diel_r,F(gg))
        *X(gg)*dt;
    P(gg)=kd(mun(gg)+mup(gg),a,diel_r,F(gg))/(kd(mun(gg)+mup(gg),
        a,diel_r,F(gg))+kf);

```

```

    U(gg)=P(gg)*G2(gg-1)/(dl*q*1000)-(1-P(gg))*R(gg);
end

p(1)=p(1)+n(2)-nnew(2);
n(1)=n(1)+p(2)-pnew(2);
p(althick+2)=p(althick+2)+n(althick+1)-nnew(althick+1);
n(althick+2)=n(althick+2)+p(althick+1)-pnew(althick+1);
xcheck(iter)=p(8);xcheck1(iter)=n(8);
if flag==1
    for gg=2:althick+1
        if abs(Xnew(gg)-X(gg))>abs(converge*dt*Xnew(gg))
            flag=0;
        end
    end
end

if flag==1
    for gg=3:althick
        if abs(pnew(gg)-p(gg))>abs(converge*dt*pnew(gg))
            flag=0;
        end
        if abs(nnew(gg)-n(gg))>abs(converge*dt*nnew(gg))
            flag=0;
        end
    end
end

if flag==1
    jp(1)=(p(2)-pnew(2))*dl*q*1000/dt;
    jn(1)=-n(2)-nnew(2))*dl*q*1000/dt;

```

```

jt(1)=jp(1)+jn(1);

jp(althick+1)=-(p(althick+1)-pnew(althick+1))*dl*q*1000/dt;
jn(althick+1)=(n(althick+1)-nnew(althick+1))*dl*q*1000/dt;
jt(althick+1)=jp(althick+1)+jn(althick+1);

if abs(jt(1)-jt(althick+1))>abs(converge*(abs(jt(althick+1))+abs(jt
    flag=0;
end

for gg=2:althick
    dpp=dt*(Dp(gg)*p(gg)-Dp(gg+1)*p(gg+1))/(dl*dl);
    jpdiff(gg)=dpp*dl*q*1000/dt;

    dpp=0;
    if(F(gg)>0)
        dpp=dt*p(gg)*mup(gg)*abs(F(gg))/dl;
    end
    if (F(gg+1)<0)
        dpp=dpp-dt*p(gg+1)*mup(gg+1)*abs(F(gg+1))/dl;
    end
    jpdrift(gg)=dpp*dl*q*1000/dt;

    dnn=dt*(Dn(gg)*n(gg)-Dn(gg+1)*n(gg+1))/(dl*dl);
    jndiff(gg)=-dnn*dl*q*1000/dt;

    dnn=0;
    if(F(gg)<0)
        dnn=dt*n(gg)*mun(gg)*abs(F(gg))/dl;
    end
    if (F(gg+1)>0)

```



```

        dnn=dnn-dt*n(gg+1)*mun(gg+1)*abs(F(gg+1))/dl;
    end
    jndrift(gg)=-dnn*dl*q*1000/dt;

    jp(gg)=jpdiff(gg)+jpdrift(gg);
    jn(gg)=jndiff(gg)+jndrift(gg);
    jt(gg)=jp(gg)+jn(gg);
end

end

for gg=3:althick
    p(gg)=pnew(gg);n(gg)=nnew(gg);
    X(gg)=Xnew(gg);
end
X(2)=Xnew(2);
X(althick+1)=Xnew(althick+1);

%Electrical Field Calculation
for mm=1:althick+1
    Fint(mm)=0;
    for pp=1:althick+2
        if pp<=mm
            Fint(mm)=Fint(mm)+dl*q*(p(pp)-n(pp))/2/diel_0/diel_r;
        else
            Fint(mm)=Fint(mm)-dl*q*(p(pp)-n(pp))/2/diel_0/diel_r;
        end
    end
end
end
for mm=2:althick+1

```

```

        F(mm)=(Fint(mm-1)+Fint(mm))/2;
    end
    VF=sum(F.*dl);
    VF=Vbi+VF;
    n(1)=n(1)+(VF-VV)*diel_0*diel_r/(q*dl*althick*dl);
    p(althick+2)=p(althick+2)+(VF-VV)*diel_0*diel_r
        /(q*dl*althick*dl);
    if n(1)<p(1)
        p(1)=p(1)-n(1);n(1)=0;
    else
        n(1)=n(1)-p(1);p(1)=0;
    end
    if n(althick+2)<p(althick+2)
        p(althick+2)=p(althick+2)-n(althick+2);n(althick+2)=0;
    else
        n(althick+2)=n(althick+2)-p(althick+2);p(althick+2)=0;
    end
    for mm=2:althick+1
        F(mm)=F(mm)-(VF-VV)/althick/dl;
        mun(mm)=mun0(mm)*exp(En0(mm)*sqrt(abs(F(mm))));
        Dn(mm)=mun(mm)*kT;
        mup(mm)=mup0(mm)*exp(Ep0(mm)*sqrt(abs(F(mm))));
        Dp(mm)=mup(mm)*kT;
    end
    x=[abs(mun.*F); abs(mup.*F);abs(Dn/dl);abs(Dp/dl)];
    mufmax=max(max(x));
    dt=dl/mufmax/ts_factor;

else break
end
end
end

```

```

if flag==0
    jp(1)=(p(2)-pnew(2))*dl*q*1000/dt;
    jn(1)=-(n(2)-nnew(2))*dl*q*1000/dt;
    jt(1)=jp(1)+jn(1);

    jp(althick+1)=-(p(althick+1)-pnew(althick+1))*dl*q*1000/dt;
    jn(althick+1)=(n(althick+1)-nnew(althick+1))*dl*q*1000/dt;
    jt(althick+1)=jp(althick+1)+jn(althick+1);

    if abs(jt(1)-jt(althick+1))>abs(converge*(abs(jt(althick+1))
        +abs(jt(1))))

        flag=0;
    end

    for gg=2:althick
        dpp=dt*(Dp(gg)*p(gg)-Dp(gg+1)*p(gg+1))/(dl*dl);
        jpdiff(gg)=dpp*dl*q*1000/dt;

        dpp=0;
        if (F(gg)>0)
            dpp=dt*p(gg)*mup(gg)*abs(F(gg))/dl;
        end
        if (F(gg+1)<0)
            dpp=dpp-dt*p(gg+1)*mup(gg+1)*abs(F(gg+1))/dl;
        end
        jpdrift(gg)=dpp*dl*q*1000/dt;

        dnn=dt*(Dn(gg)*n(gg)-Dn(gg+1)*n(gg+1))/(dl*dl);
        jndiff(gg)=-dnn*dl*q*1000/dt;
    end
end

```

```

        dnn=0;
        if(F(gg)<0)
            dnn=dt*n(gg)*mun(gg)*abs(F(gg))/dl;
        end
        if (F(gg+1)>0)
            dnn=dnn-dt*n(gg+1)*mun(gg+1)*abs(F(gg+1))/dl;
        end
        jndrift(gg)=-dnn*dl*q*1000/dt;

        jp(gg)=jpdiff(gg)+jpdrift(gg);
        jn(gg)=jndiff(gg)+jndrift(gg);
        jt(gg)=jp(gg)+jn(gg);
    end

end

power(yy)=0;
power(yy)= -VV*jt(1); Ji(yy)=jt(1); Jf(yy)=jt(althick+1);
if((VV>0) && (power(yy)>pmax))
    pmax=power(yy); Vpmax=VV; Jpmax=jt(1);
end
if(abs(VV)<1.0e-3)
    Jsc=jt(1);
end
if(VV>=0 && jt(1)<0 && abs(jt(1))<abs(Jocbot))
    Jocbot=jt(1); Vocbot=VV;
end
if(VV>=0 && jt(1)>0 && abs(jt(1))<abs(Joctop))
    Joctop=jt(1); Voctop=VV;
end
end

```

```
end
```

```
Voc=(Joctop*Vocbot-Jocbot*Voctop)/(Joctop-Jocbot);
```

```
Jsc=abs(Jsc);
```

```
FF=pmax/(Jsc*Voc);
```

```
figure(2)
```

```
plot(V, Ji(1:9));
```

Bibliography

- [1] SL Nathan, G Crabtree, AJ Nozik, MR Wasielewski, and P Alivisatos. Basic research needs for solar energy utilization. In *Report on the basic energy sciences workshop on solar energy utilization. CIO Technology*, 2005.
- [2] George W Crabtree and Nathan S Lewis. Solar energy conversion physics today, 2007.
- [3] J. Hakes. Long term world oil supply (a resource base/production path analysis), 2000.
- [4] Sarah Kurtz and John Geisz. Multijunction solar cells for conversion of concentrated sunlight to electricity. *Optics express*, 18(101):A73–A78, 2010.
- [5] Tom Key. Solar photovoltaics: Expanding electric generation options. *Electric Power Research Institute*, 2007.
- [6] Gang Yu, Jun Gao, Jan C Hummelen, Fred Wudl, and Alan J Heeger. Polymer photovoltaic cells: enhanced efficiencies via a network of internal donor-acceptor heterojunctions. *Science-AAAS-Weekly Paper Edition*, 270(5243):1789–1790, 1995.
- [7] Hsiang-Yu Chen, Jianhui Hou, Shaoqing Zhang, Yongye Liang, Guanwen Yang, Yang Yang, Luping Yu, Yue Wu, and Gang Li. Polymer solar cells with enhanced open-circuit voltage and efficiency. *Nature Photonics*, 3(11):649–653, 2009.
- [8] Serap Günes, Helmut Neugebauer, and Niyazi Serdar Sariciftci. Conjugated polymer-based organic solar cells. *Chemical reviews*, 107(4):1324–1338, 2007.

- [9] Frederik C Krebs, Thomas Tromholt, and Mikkel Jørgensen. Upscaling of polymer solar cell fabrication using full roll-to-roll processing. *Nanoscale*, 2(6):873–886, 2010.
- [10] Amal K Ghosh and Tom Feng. Merocyanine organic solar cells. *Journal of Applied Physics*, 49(12):5982–5989, 1978.
- [11] Lijun Huo, Tao Liu, Xiaobo Sun, Yunhao Cai, Alan J Heeger, and Yanming Sun. Single-junction organic solar cells based on a novel wide-bandgap polymer with efficiency of 9.7%. *Advanced Materials*, 27(18):2938–2944, 2015.
- [12] B Zimmermann, M Glatthaar, M Niggemann, MK Riede, A Hinsch, and A Gombert. Ito-free wrap through organic solar cells module concept for cost-efficient reel-to-reel production. *Solar Energy Materials and Solar Cells*, 91(5):374–378, 2007.
- [13] Nurul Bariah Idris, Mohd Natashah Norizan, and Ili Salwani Mohamad. Organic solar cell: An overview on performance and fabrication techniques. In *Applied Mechanics and Materials*, volume 754, pages 540–545. Trans Tech Publ, 2015.
- [14] LJA Koster, ECP Smits, VD Mihailetschi, and PWM Blom. Device model for the operation of polymer/fullerene bulk heterojunction solar cells. *Physical Review B*, 72(8):085205, 2005.
- [15] Thomas Kirchartz, Bart E Pieters, Kurt Taretto, and Uwe Rau. Electro-optical modeling of bulk heterojunction solar cells. *Journal of applied physics*, 104(9):094513, 2008.
- [16] Chunjun Liang, Yongsheng Wang, Dan Li, Xingchen Ji, Fujun Zhang, and Zhiqun He. Modeling and simulation of bulk heterojunction polymer solar cells. *Solar Energy Materials and Solar Cells*, 127:67–86, 2014.
- [17] Jing Han Yap, Tran Thinh To, and Stefan Adams. Monte carlo morphological modelling of a p3ht: Pcbm bulk heterojunction organic solar cell. *Journal of Polymer Science Part B: Polymer Physics*, 53(4):270–279, 2015.

-
- [18] Edmond Becquerel. *La lumière, ses causes et ses effets*. F. Didot Frères, 1867.
- [19] John Perlin. *From space to earth: the story of solar electricity*. Earthscan, 1999.
- [20] Paul M Borsenberger and David S Weiss. *Organic photoreceptors for imaging systems*, volume 39. M. Dekker New York, 1993.
- [21] C K Chiang, CR Fincher Jr, YW Park, AJ Heeger, H Shirakawa, EJ Louis, SC Gau, and Alan G MacDiarmid. Electrical conductivity in doped polyacetylene. *Physical Review Letters*, 39(17):1098, 1977.
- [22] Hideki Shirakawa, Alan McDiarmid, and Alan Heeger. Twenty-five years of conducting polymers. *Chemical Communications*, 2003(1):1–4, 2003.
- [23] Ching W Tang. Two-layer organic photovoltaic cell. *Applied Physics Letters*, 48(2):183–185, 1986.
- [24] Business Wire. Solarmer energy, inc. breaks psychological barrier with 8.13% opv efficiency, 2010.
- [25] Solar cell - generations, . URL http://en.wikipedia.org/wiki/Solar_cell#Second_Generation.
- [26] G. Gourdin. Lecture notes: Solar cell technology (current state of the art), 2007.
- [27] Martin A Green. Third generation photovoltaics: solar cells for 2020 and beyond. *Physica E: Low-dimensional Systems and Nanostructures*, 14(1):65–70, 2002.
- [28] Third generation solar cell, . URL http://en.wikipedia.org/wiki/Third_generation_solar_cell.
- [29] Sam-Shajing Sun and Niyazi Serdar Sariciftci. *Organic photovoltaics: mechanisms, materials, and devices*. CRC press, 2005.

- [30] Ruthanne Hassey, Ellen J Swain, Nathan I Hammer, Dhandapani Venkataraman, and Michael D Barnes. Probing the chiroptical response of a single molecule. *Science*, 314(5804):1437–1439, 2006.
- [31] Bernard Kippelen and Jean-Luc Brédas. Organic photovoltaics. *Energy & Environmental Science*, 2(3):251–261, 2009.
- [32] Jean-Luc Brédas, Joseph E Norton, Jérôme Cornil, and Veaceslav Coropceanu. Molecular understanding of organic solar cells: the challenges. *Accounts of chemical research*, 42(11):1691–1699, 2009.
- [33] H Neugebauer, C Brabec, JC Hummelen, and NS Sariciftci. Stability and photodegradation mechanisms of conjugated polymer/fullerene plastic solar cells. *Solar Energy Materials and Solar Cells*, 61(1):35–42, 2000.
- [34] Frederik C Krebs, Jon E Carlé, Nicolaj Cruys-Bagger, Morten Andersen, Mathilde R Lilliedal, Mark A Hammond, and Søren Hvidt. Lifetimes of organic photovoltaics: photochemistry, atmosphere effects and barrier layers in ito-mehppv: Pcbm-aluminium devices. *Solar Energy Materials and Solar Cells*, 86(4):499–516, 2005.
- [35] Pallavi Madakasira, Kanzan Inoue, Ross Ulbricht, Sergey B Lee, M Zhou, John P Ferraris, and Anvar A Zakhidov. Multilayer encapsulation of plastic photovoltaic devices. *Synthetic Metals*, 155(2):332–335, 2005.
- [36] William J Potscavage Jr, SeungHyup Yoo, Benoit Domercq, and Bernard Kippelen. Encapsulation of pentacene/ c_{60} organic solar cells with al_2o_3 deposited by atomic layer deposition. 2007.
- [37] C Waldauf, M Morana, P Denk, P Schilinsky, K Coakley, SA Choulis, and CJ Brabec. Highly efficient inverted organic photovoltaics using solution based titanium oxide as electron selective contact. *Applied Physics Letters*, 89(23):233517, 2006.

- [38] MS White, DC Olson, SE Shaheen, N Kopidakis, and David S Ginley. Inverted bulk-heterojunction organic photovoltaic device using a solution-derived zno underlayer. *Applied Physics Letters*, 89(14):143517, 2006.
- [39] G Dennler, C Lungenschmied, H Neugebauer, NS Sariciftci, and A Labouret. Flexible, conjugated polymer-fullerene-based bulk-heterojunction solar cells: basics, encapsulation, and integration. *Journal of materials research*, 20(12):3224–3233, 2005.
- [40] Jay S Lewis and Michael S Weaver. Thin-film permeation-barrier technology for flexible organic light-emitting devices. *Selected Topics in Quantum Electronics, IEEE Journal of*, 10(1):45–57, 2004.
- [41] Chih-Yu Chang, Chun-Ting Chou, Yun-Jun Lee, Miin-Jang Chen, and Feng-Yu Tsai. Thin-film encapsulation of polymer-based bulk-heterojunction photovoltaic cells by atomic layer deposition. *Organic Electronics*, 10(7):1300–1306, 2009.
- [42] URL <http://rredc.nrel.gov/solar/spectra/am1.5/>.
- [43] LJA Koster, ECP Smits, VD Mihailetschi, and PWM Blom. Device model for the operation of polymer/fullerene bulk heterojunction solar cells. *Physical Review B*, 72(8):085205, 2005.
- [44] VD Mihailetschi, LJA Koster, JC Hummelen, and PWM Blom. Photocurrent generation in polymer-fullerene bulk heterojunctions. *Physical review letters*, 93(21):216601, 2004.
- [45] Paul WM Blom, Valentin D Mihailetschi, L Jan Anton Koster, and Denis E Markov. Device physics of polymer: fullerene bulk heterojunction solar cells. *Advanced Materials*, 19(12):1551–1566, 2007.
- [46] MM Chowdhury and MK Alam. An optoelectronic analytical model for bulk heterojunction organic solar cells incorporating position and wavelength dependent carrier generation. *Solar Energy Materials and Solar Cells*, 132:107–117, 2015.

- [47] Biswajit Ray, Camila Andrea Gonzalez Williamson, Mohammad Ryyan Khan, and Muhammad A. Alam. Opv lab, Oct 2011. URL <https://nanohub.org/resources/12187>.
- [48] H Bässler. Charge transport in disordered organic photoconductors, a monte carlo simulation study. *phys. stat. sol.(b)* 175. 1993.
- [49] Amal K Ghosh and Tom Feng. Merocyanine organic solar cells. *Journal of Applied Physics*, 49(12):5982–5989, 1978.
- [50] Haichao Duan, Junliang Yang, Lin Fu, Jian Xiong, Bingchu Yang, Jun Ouyang, Conghua Zhou, Han Huang, and Yongli Gao. Interface modification of organic photovoltaics by combining molybdenum oxide (moox) and molecular template layer. *Thin Solid Films*, 574:146–151, 2015.
- [51] Fan Yang, Max Shtein, and Stephen R Forrest. Controlled growth of a molecular bulk heterojunction photovoltaic cell. *Nature Materials*, 4(1):37–41, 2005.
- [52] Peter Peumans, Soichi Uchida, and Stephen R Forrest. Efficient bulk heterojunction photovoltaic cells using small-molecular-weight organic thin films. *Nature*, 425(6954):158–162, 2003.
- [53] Lijun Huo, Tao Liu, Xiaobo Sun, Yunhao Cai, Alan J Heeger, and Yanming Sun. Single-junction organic solar cells based on a novel wide-bandgap polymer with efficiency of 9.7%. *Advanced Materials*, 27(18):2938–2944, 2015.
- [54] B Zimmermann, M Glatthaar, M Niggemann, MK Riede, A Hinsch, and A Gombert. Ito-free wrap through organic solar cells a module concept for cost-efficient reel-to-reel production. *Solar Energy Materials and Solar Cells*, 91(5):374–378, 2007.
- [55] Nurul Bariah Idris, Mohd Natashah Norizan, and Ili Salwani Mohamad. Organic solar cell: An overview on performance and fabrication techniques. In *Applied Mechanics and Materials*, volume 754, pages 540–545. Trans Tech Publ, 2015.

- [56] Gilles Dennler, Markus C Scharber, Christoph J Brabec, et al. Polymer-fullerene bulk-heterojunction solar cells. *Adv. Mater*, 21(13):1323–1338, 2009.
- [57] Myungsun Sim, Jisoo Shin, Chiyeoung Shim, Min Kim, Sae Byeok Jo, Joo-Hyun Kim, and Kilwon Cho. Dependence of exciton diffusion length on crystalline order in conjugated polymers. *The Journal of Physical Chemistry C*, 118(2):760–766, 2014.
- [58] Gang Yu, Jun Gao, Jan C Hummelen, Fred Wudl, and Alan J Heeger. Polymer photovoltaic cells: enhanced efficiencies via a network of internal donor-acceptor heterojunctions. *Science-AAAS-Weekly Paper Edition*, 270(5243):1789–1790, 1995.
- [59] Michael D Irwin, D Bruce Buchholz, Alexander W Hains, Robert PH Chang, and Tobin J Marks. p-type semiconducting nickel oxide as an efficiency-enhancing anode interfacial layer in polymer bulk-heterojunction solar cells. *Proceedings of the National Academy of Sciences*, 105(8):2783–2787, 2008.
- [60] Valentin D Mihailetschi, L Jan Anton Koster, Paul WM Blom, Christian Melzer, Bert de Boer, Jeroen KJ van Duren, and René AJ Janssen. Compositional dependence of the performance of poly (p-phenylene vinylene):methanofullerene bulk-heterojunction solar cells. *Advanced Functional Materials*, 15(5):795–801, 2005.
- [61] Eiji Itoh, Yasutake Maruyama, and Katsutoshi Fukuda. Photovoltaic properties of bulk-heterojunction organic solar cell with ultrathin titanium oxide nanosheet as electron selective layer. *Japanese Journal of Applied Physics*, 52(4S):04CK05, 2013.
- [62] Chunjun Liang, Yongsheng Wang, Dan Li, Xingchen Ji, Fujun Zhang, and Zhiqun He. Modeling and simulation of bulk heterojunction polymer solar cells. *Solar Energy Materials and Solar Cells*, 127:67–86, 2014.
- [63] Leif AA Pettersson, Lucimara S Roman, and Olle Inganäs. Modeling photocurrent action spectra of photovoltaic devices based on organic thin films. *Journal of Applied Physics*, 86(1):487, 1999.

- [64] Peter Peumans, Aharon Yakimov, and Stephen R Forrest. Small molecular weight organic thin-film photodetectors and solar cells. *Journal of Applied Physics*, 93(7):3693–3723, 2003.
- [65] Chunfu Zhang, Dazheng Chen, Yue Hao, Zhenhua Lin, and Zhizhe Wang. *Investigation of Organic Bulk Heterojunction Solar Cells from Optical Aspect*. INTECH Open Access Publisher, 2013.
- [66] Charles L Braun. Electric field assisted dissociation of charge transfer states as a mechanism of photocarrier production. *The Journal of chemical physics*, 80(9):4157–4161, 1984.
- [67] Florent Monestier, Jean-Jacques Simon, Philippe Torchio, Ludovic Escoubas, François Flory, Sandrine Bailly, Remi de Bettignies, Stephane Guillerez, and Christophe Defranoux. Modeling the short-circuit current density of polymer solar cells based on p3ht: Pcbm blend. *Solar energy materials and solar cells*, 91(5):405–410, 2007.
- [68] Douglas W Sievers, Vishal Shrotriya, and Yang Yang. Modeling optical effects and thickness dependent current in polymer bulk-heterojunction solar cells. *Journal of applied physics*, 100(11):114509, 2006.
- [69] Pankaj Kumar, SC Jain, Vikram Kumar, Suresh Chand, and RP Tandon. A model for the jv characteristics of p3ht: Pcbm solar cells. *Journal of Applied Physics*, 105(10):104507–1, 2009.
- [70] DH Dunlap, PE Parris, and VM Kenkre. Charge-dipole model for the universal field dependence of mobilities in molecularly doped polymers. *Physical review letters*, 77(3):542, 1996.
- [71] HCF Martens, PWM Blom, and HFM Schoo. Comparative study of hole transport in poly (p-phenylene vinylene) derivatives. *Physical Review B*, 61(11):7489, 2000.
- [72] Murray A Lampert and Peter Mark. *Current injection in solids*. Academic Press, 1970.

- [73] Siegfried Selberherr. *Analysis and simulation of semiconductor devices*. Springer Science & Business Media, 2012.
- [74] P Langevin. Sur la loi de recombinaison des ions. *Ann. Chim. Phys*, 28: 433–530, 1903.
- [75] George F Burkhard, Eric T Hoke, and Michael D McGehee. Accounting for interference, scattering, and electrode absorption to make accurate internal quantum efficiency measurements in organic and other thin solar cells. *Advanced Materials*, 22(30):3293–3297, 2010.
- [76] Astm, astmg 173-03 tables:extraterrestrial spectrum, terrestrial global 37 deg south facing tilt & direct normal circumsolar. [.http://rredc.nrel.gov/solar/spectra/am1.5/..](http://rredc.nrel.gov/solar/spectra/am1.5/) [Online; Available].
- [77] Gang Li, Vishal Shrotriya, Yan Yao, and Yang Yang. Investigation of annealing effects and film thickness dependence of polymer solar cells based on poly(3-hexylthiophene). *Journal of Applied Physics*, 98(4):043704, 2005.
- [78] Young Min Nam, June Huh, and Won Ho Jo. Optimization of thickness and morphology of active layer for high performance of bulk-heterojunction organic solar cells. *Solar Energy Materials and Solar Cells*, 94(6):1118–1124, 2010.
- [79] Douglas W Sievers, Vishal Shrotriya, and Yang Yang. Modeling optical effects and thickness dependent current in polymer bulk-heterojunction solar cells. *Journal of applied physics*, 100(11):114509, 2006.
- [80] Minas M Stylianakis and Emmanuel Kymakis. Efficiency enhancement of organic photovoltaics by addition of carbon nanotubes into both active and hole transport layer. *Applied Physics Letters*, 100(9):093301, 2012.
- [81] Liming Liu, William E Stanchina, and Guangyong Li. Enhanced performance of bulk heterojunction solar cells fabricated by polymer: Fullerene: Carbon-nanotube composites. In *Nanotechnology, 2008. NANO'08. 8th IEEE Conference on*, pages 233–236. IEEE, 2008.

- [82] Solenn Berson, Rémi de Bettignies, Severine Bailly, Stephane Guillerez, and Bruno Jousselme. Elaboration of p3ht/cnt/pcbm composites for organic photovoltaic cells. *Advanced Functional Materials*, 17(16):3363–3370, 2007.
- [83] Florent Monestier, Jean-Jacques Simon, Philippe Torchio, Ludovic Escoubas, Bernard Ratier, Wassim Hojeij, Bruno Lucas, André Moliton, Michel Cathelinaud, Christophe Defranoux, et al. Optical modeling of organic solar cells based on cupc and c 60. *Applied optics*, 47(13):C251–C256, 2008.
- [84] H Looyenga. Dielectric constants of heterogeneous mixtures. *Physica*, 31(3):401–406, 1965.
- [85] Rajendra R Zope, Tunna Baruah, Mark R Pederson, and BI Dunlap. Static dielectric response of icosahedral fullerenes from c 60 to c 2160 characterized by an all-electron density functional theory. *Physical Review B*, 77(11):115452, 2008.
- [86] AP Marchetti, KE Sassin, RH Young, LJ Rothberg, and DY Kondakov. Integer charge transfer states in organic light-emitting diodes: Optical detection of hole carriers at the anode— organic interface. *Journal of Applied Physics*, 109(1):3709, 2011.
- [87] M Magdalena Mandoc, Welmoed Veurman, L Jan Anton Koster, Bert de Boer, and Paul WM Blom. Origin of the reduced fill factor and photocurrent in mdmo-ppv: Pcnev all-polymer solar cells. *Advanced Functional Materials*, 17(13):2167–2173, 2007.